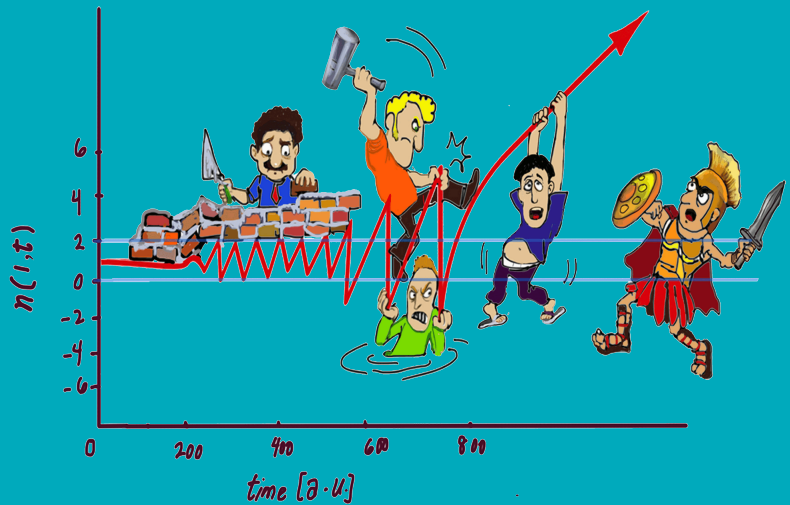# Electronic structure and transport from density matrices and density functionals

Javad Hashemi

Electronic structure and transport from density matrices and density functionals

Javad Hashemi

A doctoral dissertation completed for the degree of Doctor of Science in Technology to be defended, with the permission of the Aalto University School of Science, at a public examination held at the lecture hall E of the school on 14th of December 2012 at 13 o'clock.

Aalto University
School of Science
Department of Applied Physics
COMP/EPM

Supervising professor
Prof. Risto Nieminen

Preliminary examiners
Prof. Esa Räsänen, Tampere University of Technology, Finland
Prof. Kristian Sommer Thygesen, Technical University of Denmark,
Denmark

Opponent
Prof. Stefano Sanvito, Trinity College Dublin, Ireland

NORDIC ECOLABEL

441   697
Printed matter

Abstract

  As a link between theory and experiment, computational physics has received increasing attention in the last decades. Powerful supercomputers provide the possibility of accurate calculations for large systems, while highly advanced experimental tools allow researchers to conduct experiments on mesoscopic scale. Such developments lead to a bigger overlap area between these two fields of physics.

On the other hand, computational approaches are based on theories that are under constant enhancement in order to obtain more accurate results, and therefore, both application and theory development have crucial role in this field of physics. In the present dissertation, we contribute to the both parts.

  In the first part, we apply the density functional approach on carbon-nanotube-based systems, and we study the effect of defects addatoms, impurities, and their periodicity on the electronic transport properties of the systems. We also predict the formation of Schottky barrier in the junction between two metallic and semiconducting nanotubes. The second part is dedicated to study the challenges and difficulties in time dependent reduced density matrix approaches. We show that the current approximations make the time evolution of two-body reduced density matrix very unstable. We study the possible reasons behind such behavior, and this might lead us to more stable approximations.

Preface

Particles do interact and that interaction usually is not negligible. This is one of the very basic things that physics teaches us. However, to know the importance of human interaction, we don't really need physics. Our daily experiences tell it loud and clear. I highly value my constructive interactions during the period of my doctoral studies. It was not an easy journey to take it alone.

I am very thankful to Professor Risto Nieminen for his supports and encouragements during the time of my studies. I am also grateful to Prof. Martti Puska, Prof. Angel Rubio, and Prof. Robert van Leeuwen for our useful collaborations. Our discussions were, at many points, enlightening and fruitful and enhanced my understanding. I also learned a lot from my old friend and recent collaborator Dr. Ali Akbari; I am happy about and grateful for our collaboration and more importantly our friendship.

Quite often, I feel very lucky and happy for having amazing friends. Those who stand by your side in failure and success. I am thankful to them, now and ever, for making my life better.

During these years, I was working in a very relaxing atmosphere and I had very friendly and helpful colleagues. Moreover, we had an excellent lunch group that made up for the food quality. Many thanks to all of them.

Special thanks to Pezhman Behjouyan for his creative work for the cover.

I dedicate this work to my family. They are my real treasure in life, their support is priceless and their care and kindness is endless.

Helsinki, November 15, 2012,

Javad Hashemi

Contents

List of Publications

This thesis consists of an overview and of the following publications which are referred to in the text by their Roman numerals.

I J. A. Fürst, J. Hashemi, T. Markussen, M. Brandbyge, A. P. Jauho, and R. M. Nieminen. **Electronic transport properties of fullerene functionalized carbon nanotubes: Ab initio and tight-binding calculations**. *Physical Review B*, **80**, 035427, 2009.

II M. J. Hashemi, K. Sääskilahti, and M. J. Puska. **Local semiconducting transition in armchair carbon nanotubes: The effect of periodic bi-site perturbation on electronic and transport properties of carbon nanotubes**. *Physical Review B*, **83**, 115411, 2011.

III P. Havu, M. J. Hashemi, M. Kaukonen, E. T. Seppälä, and R. M. Nieminen. **Effect of gating and pressure on the electronic transport properties of crossed nanotube junctions: formation of a Schottky barrier**. *Journal of Physics: Condensed Matter*, **23**, 112203, 2011.

IV A. Akbari, M. J. Hashemi, A. Rubio, R. M. Nieminen, and R. van Leeuwen. **Challenges in truncating the hierarchy of time-dependent reduced density matrices equations**. *Physical Review B*, **85**, 235121, 2012.

Author's Contribution

Publication I: "Electronic transport properties of fullerene functionalized carbon nanotubes: Ab initio and tight-binding calculations"

The author provided some of the ideas, performed most of the DFT calculations and analysis and prepared the first manuscript.

Publication II: "Local semiconducting transition in armchair carbon nanotubes: The effect of periodic bi-site perturbation on electronic and transport properties of carbon nanotubes"

The author provided the core ideas, performed all the calculations and analysis and wrote the paper with input from the coauthors.

Publication III: "Effect of gating and pressure on the electronic transport properties of crossed nanotube junctions: formation of a Schottky barrier"

The author provided some of the ideas, and made a major contribution to the analysis and the writing of paper.

Publication IV: "Challenges in truncating the hierarchy of time-dependent reduced density matrices equations"

The author was one of the main contributors to the idea development, analyses and writing process along with the other leading author.

1. Introduction to the electronic structure calculation methods

First half of the twentieth century gave birth to one of the greatest revolutions in the history of science. At the end of nineteenth century and beginning of twentieth, there were many experiments, in the atomic scale, that were in obvious conflict with the classical theories of mechanics and electrodynamics. The increasing discrepancies between these theories and experiments forced scientists to rethink the basic concepts and laws of physics, and led to the revolutionary theory of quantum physics or quantum mechanics. This was also called wave mechanics at the beginning since as one of the main concepts, it describes particles as waves and therefore all characteristics of an entire physical system can be explained by a wave function. Schrödinger found that the wave function changes according to a partial differential equation which is now called Schrödinger equation. It reads

$$i\hbar \, \partial_t \, \Phi(\mathbf{r}_1 \ldots \mathbf{r}_N, t) = \hat{H} \, \Phi(\mathbf{r}_1 \ldots \mathbf{r}_N, t), \qquad (1.1)$$

where Φ is the wave function, $\hat{H}$ is the Hamiltonian of the system, $\hbar$ is the reduced Plank constant, and N is the number of particles in the system. Although the Schrödinger equation contains all information about a physical system, it is practically impossible to solve for more than a few particles, and therefore we should find some approaches to simplify the equation. The effort in this direction can be categorized in the field of computational physics. Computational physics works as a link between theory and experiment because it provides a better understanding of the physical phenomena happening in an experiment by simulating similar systems and analyzing the outcomes, and it enhances both theory and experiment.

In the present dissertation, we deal with two approaches for calculating the electronic structures of materials, namely, density-functional theory (DFT) and density-matrix theory. They are both among the most powerful,

and widely used techniques to handle systems with a few to a few hundred atoms. In this chapter we briefly introduce these two techniques.

First, we will talk about density-functional theory, and then we will introduce the concept of a density matrix and discuss density-matrix-based methods for electronic structure calculations. In the rest of this chapter, we employ atomic units (a.u.), $1/(4\pi\varepsilon_0) = e^2 = \hbar = m_e = 1$, unless stated otherwise.

1.1 Density-functional theory

One of the most popular quantum physical methods to calculate the electronic structure of a system is density-functional theory (DFT). The core idea of DFT is that all time-independent observables of a many-body system can, in principle, be written as some functional of its ground-state electronic density, and therefore, the density alone is sufficient to calculate all the electronic properties of the system.

Let us consider a system with N identical particles. The time-independent Schrödinger equation for such a system reads

$$\Big[\sum_{i=1}^{N}\Big(-\frac{1}{2}\nabla^2 + v(\mathbf{r}_i)\Big) + \frac{1}{2}\sum_{i\neq j}^{N} U_{ij}\Big]\Phi(\mathbf{r}_1\ldots\mathbf{r}_N) = E\,\Phi(\mathbf{r}_1\ldots\mathbf{r}_N), \qquad (1.2)$$

where the energy operators are separately shown as

$$
\begin{aligned}
\hat{T} &= -\sum_{i=1}^{N}\tfrac{1}{2}\nabla^2, \\
\hat{V} &= \sum_{i=1}^{N} v(\mathbf{r}_i), \\
\hat{U} &= \tfrac{1}{2}\sum_{i\neq j}^{N} U_{ij}.
\end{aligned}
\qquad (1.3)
$$

Here, $v(\mathbf{r})$ is the time-independent external potential, and $U_{ij} \equiv U(\mathbf{r}_i\mathbf{r}_j)$ is the two-particle interaction which is usually spin independent and has the form $U(\mathbf{r}_i\,\mathbf{r}_j) = w(|\mathbf{r}_i - \mathbf{r}_j|)$.

In 1964 Hohenberg and Kohn [1] proved that if the ground-state density $n_0(\mathbf{r})$ of a system is known, in principle, we can obtain its ground-state wave function Φ_0; that is to say, $\Phi_0 \equiv \Phi_0[n_0]$. As a result, all the ground-state expectation values become also some functionals of $n_0(\mathbf{r})$. While already this is a profound statement, they extended the theorem and showed that we can find uniquely the external potential $v(\mathbf{r})$ of the system from the density $n_0(\mathbf{r})$, and determine the total Hamiltonian of the system (assuming we know the form of $U(\mathbf{r}_1\mathbf{r}_2)$). On the other hand, all the properties of the system are determined once the Hamiltonian is

specified. This implies that $n_0(\mathbf{r})$ characterizes in principle all properties of the system, and every observable of the system is some functional of the ground-state density.

There is also an important variational principle associated with the Hohenberg-Kohn theorem. Since the expectation value of any observable of a system is a unique functional of the ground-state density, we can certainly apply it to the ground-state energy. We can construct this functional as

$$E[n] \equiv \langle \Phi_0[n]|T + V + U|\Phi_0[n]\rangle, \tag{1.4}$$

where V is the specific external potential of a system with ground-state density $n_0(\mathbf{r})$ and ground-state energy E_0. For the case where the density $n(\mathbf{r})$ equals the ground-state density $n_0(\mathbf{r})$ corresponding to the external potential V, the functional $E[n]$ then takes on the value E_0. Since the ground-state energy is determined uniquely by $n_0(\mathbf{r})$, the Rayleigh-Ritz principle establishes that

$$E_0 < E[n] \quad \text{for } n \neq n_0. \tag{1.5}$$

This property means that we can vary the density to minimize the energy, provided we know the form of the functional $\varepsilon[n]$, or at least have a good approximation for it. In fact, we can write the ground-state energy functional in Eq. (1.4) as

$$E_{HK}[n] = F_{HK}[n] + \int v(\mathbf{r})n(\mathbf{r})\, d\mathbf{r}, \tag{1.6}$$

where $F_{HK}[n] = \langle \Phi_0[n]|T + U|\Phi_0[n]\rangle$ is a unique functional. By that we mean that $F_{HK}[n]$ is the same functional of the density $n(\mathbf{r})$ for *all* interacting systems of these N-identical particles. We thus need to determine it only once, and can then apply it to all systems.

Despite such an attractive possibility, it is important to emphasize that the Hohenberg-Kohn theorem only proves the existence of these functionals, but it does not show us a way to find the form of the functionals. In order to bypass this problem, later Kohn and Sham [2] showed that there exists a fictitious system of non-interacting electrons with the exact same ground-state density as the actual physical system. For this auxiliary system, we must solve a set of single-particle equations, called Kohn-Sham (KS) equations [2], which compare to the original interacting system, is enormously easier to solve. The Schrödinger equation for this auxiliary system reads

$$\left[-\frac{1}{2}\nabla^2 + v_{eff}(\mathbf{r})\right]\phi_i(\mathbf{r}) = \epsilon_i\,\phi_i(\mathbf{r}), \tag{1.7}$$

where

$$v_{eff}(\mathbf{r}) = v(\mathbf{r}) + v_H(\mathbf{r}) + v_{xc}(\mathbf{r}), \qquad (1.8)$$

$$v_H(\mathbf{r}) = \int d\mathbf{r}' \frac{n(\mathbf{r}')}{|\mathbf{r} - \mathbf{r}'|}, \qquad (1.9)$$

$$v_{xc}(\mathbf{r}) = \frac{\delta E_{xc}[n(\mathbf{r})]}{\delta n(\mathbf{r})}, \qquad (1.10)$$

and ϕ_i are single-particle Kohn-Sham orbitals that reproduce the single-particle density $n_s(\mathbf{r})$, which by definition is equal to the actual density of the system,

$$n(\mathbf{r}) \equiv n_s(\mathbf{r}) = \sum_{i=1}^{N} |\phi_i(\mathbf{r})|^2. \qquad (1.11)$$

Equation 1.8 tells that the effective potential of the KS system $v_{eff}(\mathbf{r})$ consists of the external potential $v(\mathbf{r})$, the Hartree potential $v_H(\mathbf{r})$, and the exchange-correlation potential $v_{xc}(\mathbf{r})$.

All the information about many-body effects of the actual physical system is encapsulated in the $v_{xc}(\mathbf{r})$, but the exact functional form of the exchange-correlation energy is not known and therefore we need to approximate it. There are many different approximation for the $E_{xc}[n(\mathbf{r})]$, but the two most popular sets of approximations are local density approximation (LDA) and generalized gradient approximation (GGA) which have the general form of

$$E_{xc}^{LDA} = \int d(\mathbf{r})n(\mathbf{r})\varepsilon_{xc}(\mathbf{r}), \qquad (1.12)$$

$$E_{xc}^{GGA} = \int d(\mathbf{r})f\big(n(\mathbf{r}), \nabla n(\mathbf{r})\big), \qquad (1.13)$$

where $\varepsilon_{xc}(\mathbf{r})$ an xc-energy density.

In this dissertation, we only use the GGA form of the xc-energy which was proposed by Perdew, Burke, and Ernzerhof (PBE) [3].

1.2 Density-matrix theory

Another approach to the electronic structure calculations has the concept of density matrix in its core. The density matrix of a quantum system is a matrix which describes the system as probability distribution of an ensemble of quantum states. The full density matrix is an alternative to the many-body wave function of the system and carries all the information hidden in it, however, reduced density matrices (RDMs) encapsulate the information by integrating over a number of spin-state coordinates and, of course, in this process some of the informations will be lost.

Before we get to the mathematical description of above-mentioned concepts, and in order to have a compact notation, we introduce two collections of space-spin coordinates as

$$X_n \equiv (\mathbf{x}_1 \ldots \mathbf{x}_n) \quad ; \quad \breve{X}_n \equiv (\mathbf{x}_{n+1} \ldots \mathbf{x}_N). \tag{1.14}$$

In this notation, $\Phi(X_N, t)$ denotes the normalized wave function of the system.

For the N-particle system the time-dependent Hamiltonian is

$$\hat{H}_{1\ldots N}(t) = \sum_{i=1}^{N} \hat{h}_i + \frac{1}{2} \sum_{i \neq j}^{N} U_{ij}, \tag{1.15}$$

where $\mathbf{x}$ includes both space coordinates $\mathbf{r}$ and spin coordinates σ of the particles. The one-body part, $\hat{h}_i \equiv \hat{h}(\mathbf{x}_i, t)$, will be time-dependent and of the form

$$h(\mathbf{x}, t) = -\frac{1}{2}\nabla^2 + v(\mathbf{x}, t), \tag{1.16}$$

where v is a general time-dependent external field.

Now, we can define the density matrix for such a system as

$$\Gamma^{(N)}(X_N, X_N', t) = N! \, \Phi(X_N, t) \, \Phi^*(X_N', t). \tag{1.17}$$

This matrix contains exactly the same information as the full wave function of the system. However, as we will show shortly, for most of the observables we deal with, e.g. the total energy, we only need a part of the embedded information in the density matrix. This reduced information can be restored in the reduced density matrices. We define an n-body reduced density matrix, $\Gamma^{(n)}$, as

$$\Gamma^{(n)}(X_n, X_n', t) = \frac{N!}{(N-n)!} \int d\breve{X}_n \, \Phi(X_n, \breve{X}_n, t) \, \Phi^*(X_n', \breve{X}_n, t), \tag{1.18}$$

where $d\breve{X}_n \equiv d\mathbf{x}_{n+1} \ldots d\mathbf{x}_N$ and $\int d\mathbf{x} = \sum_\sigma \int d\mathbf{r}$.

This object contains the full information of (up to) n-body interactions in the system. Based on above definitions, several important properties of RDMs follow.

1. One can easily show from Eq. (1.18) that for an n-body operator, $\hat{A}^{(n)}$, the expectation value can be calculated as

$$< \hat{A}^{(n)} > = Tr(A^{(n)}\Gamma^{(n)}) \tag{1.19}$$

and therefore it is enough to have access to the $\Gamma^{(n)}$ instead of full density matrix or many-body wave function.

2. Different levels of RDMs are connected to each other by the equation

$$\int d\mathbf{x}_{n+1}\, \Gamma^{(n+1)}(X_n\mathbf{x}_{n+1}, X'_n\mathbf{x}_{n+1}, t) = (N-n)\, \Gamma^{(n)}(X_n, X'_n, t), \qquad (1.20)$$

which we refer to it as *partial trace relation*. Consequently, if $\Gamma^{(n)}$ is available, all RDMs with lower order can be calculated straightforwardly.

3. Equation (1.18) implies that all RDMs are positive-semidefinite which refers to the fact that all eigenvalues of RDMs are always equal to or greater than zero. For a given order RDM, these eigenvalues and their corresponding eigenvectors can be calculated as

$$\int dX'_n\, \Gamma^{(n)}(X_n, X'_n, t)\, g_i(X'_n, t) = \lambda_i(t)\, g_i(X_n, t), \quad \lambda_i(t) \geq 0. \qquad (1.21)$$

Conventionally, the eigenvectors and eigenvalues of $\Gamma^{(1)}$ are called natural orbitals and natural orbital occupation numbers, and of $\Gamma^{(2)}$ are called geminals and geminal occupation numbers, respectively.

4. In the case of fermionic particles, the Pauli exclusion principle enforces natural orbital occupation numbers to be less than or equal to one [4]. Thus, they have to remain between zero and one. This is what we call the *fermionic inequality* in this work.

5. The diagonal of $\Gamma^{(1)}$ is the electronic density, and therefore, its trace will add up to the number of particles N.

The later property suggests that we can use $\Gamma^{(1)}$ as a central variable to calculate the physical quantities of a quantum system. That leads to what is known as *reduced density matrix functional theory* (RDMFT). As an advantage in RDMFT, by having $\Gamma^{(1)}$, we immediately can calculate all one-body observables (Eq. 1.19), while in DFT, the density functional form of observables are not generally known.

Nevertheless, for other n-body observables ($n \geq 2$), we need to approximate $\Gamma^{(n)}$ as a functional of $\Gamma^{(1)}$.

1.2.1   Ground-state method: RDMFT*

As we stated in the previous section, Hohenberg and Kohn proved that, apart from the one to one relation between $n_0(r)$ and Φ_0, we can determine

---

*In this section we ignore the spin coordinates for simplicity.

uniquely $v(\mathbf{r})$ from the ground-state density $n_0(r)$, and this means that we can calculate all the time-independent properties of the system with knowledge of the ground-state density alone. However, when the external potential is spin dependent [5] or nonlocal, many external potentials yield the same ground state, and thus, the relation between $v(\mathbf{r})$ and Φ_0 is not one to one any longer. Although this implies that for these systems, the density does not determine (even in principle) all the properties of the system, what we need in practice from the Hohenberg-Kohn theorem is only the existence of the one to one relation between Φ_0 and the density, which permits us to write the functional relation $E[n]$ and define a universal functional. Thus, we must investigate how the presence of nonlocal external potentials affects the one to one relation between Φ_0 and $n_0(\mathbf{r})$. This analysis was done initially by Gilbert [6], and is usually referred to as the Gilbert theorem. The theorem states that there exists a one to one mapping between the ground-state wave function Φ_0 and the one-body reduced density matrix $\Gamma_0^{(1)}(\mathbf{r},\mathbf{r}')$, and therefore the ground-state density $n_0(r)$.

The Gilbert theorem also suggests that we can use $\Gamma_0^{(1)}(\mathbf{r},\mathbf{r}')$ for calculating the ground-state properties of a physical system. As and advantage to DFT, here we know the exact functional form of single-particle energy terms, which is very encouraging. This is a direct outcome of the relation (1.19); in fact, this also enables us to calculate all one-body observables once $\Gamma^{(1)}$ is given. In a similar fashion to $E_{HK}[n]$, we can define the energy functional

$$E[\Gamma^{(1)}] = \int \left[-\frac{1}{2}\delta(\mathbf{r} - \mathbf{r}')\nabla_{\mathbf{r}'}^2 + v(\mathbf{r},\mathbf{r}') \right]\Gamma^{(1)}(\mathbf{r},\mathbf{r}')\,d\mathbf{r}\,d\mathbf{r}' + U[\Gamma^{(1)}], \quad (1.22)$$

where

$$U[\Gamma^{(1)}] = \langle \Psi[\Gamma^{(1)}]|U|\Psi[\Gamma^{(1)}]\rangle = \frac{1}{2}\,\mathbf{Tr}(U\,\Gamma^{(2)}[\Gamma^{(1)}]). \quad (1.23)$$

As in DFT, here we can also minimize this energy functional to find the ground-state energy and one-body RDM $\Gamma_0^{(1)}$. In order to do that, we must approximate the two-body RDM in Eq. (1.23). Over the last decade, many approximations have been developed [7–22, 22–24] where one can employ for the minimization. However, we drop the discussion about their qualities and refer to [25] for more information.

1.2.2 Time evolution: The BBGKY Hierarchy

Having the equation of motion for n-RDMs enables us to study the dynamical properties of all n-body operator. Such an equation can be derived by

combining the time-dependent Schrödinger equation and time-derivative of Eq. (1.18) so that we have

$$
i\partial_t\Gamma^{(n)}(X_n, X_n', t) = \frac{N!}{(N-n)!}\int d\breve{X}_n\Big([\hat{H}_{1...N}\Phi(X_n, \breve{X}_n, t)]\Phi^*(X_n', \breve{X}_n, t) \\
-\Phi(X_n, \breve{X}_n, t)[\hat{H}_{1'...n',n+1...N}\Phi^*(X_n', \breve{X}_n, t)]\Big). \quad (1.24)
$$

Now, we split $\hat{H}_{1...N}$ into three parts. A part depending only on coordinates $1...n$, an other part depending only on coordinates $n+1...N$ and a coupling term between the coordinates of these two parts, i.e.

$$
\hat{H}_{1...N} = \hat{H}_{1...n} + \hat{H}_{n+1...N} + \sum_{i=1}^{n}\sum_{j=n+1}^{N} U_{ij}. \quad (1.25)
$$

Replacing $\hat{H}_{1...N}$ and $\hat{H}_{1'...n',n+1...N}$, in the Eq. (1.24), by Eq. (1.25) we have

$$
\begin{aligned}
i\partial_t\Gamma^{(n)}(X_n, X_n', t) = & (\hat{H}_{1...n} - \hat{H}_{1'...n'})\Gamma^{(n)} \\
& +\frac{N!}{(N-n)!}\int d\breve{X}_n\Big([\hat{H}_{n+1...N}\Phi(X_n, \breve{X}_n, t)]\Phi^*(X_n', \breve{X}_n, t) \\
& -\Phi(X_n, \breve{X}_n, t)[\hat{H}_{n+1...N}\Phi^*(X_n', \breve{X}_n, t)]\Big) \\
& +\frac{N!}{(N-n)!}\sum_{i=1}^{n}\sum_{j=n+1}^{N}\int d\breve{X}_n\Big([U(\mathbf{x}_i\mathbf{x}_{n+1}) - U(\mathbf{x}_i'\mathbf{x}_{n+1})] \\
& \Phi(X_n, \breve{X}_n, t)\Phi^*(X_n', \breve{X}_n, t)\Big), \quad (1.26)
\end{aligned}
$$

where the second term on the righthand side is zero due to the Hermicity of $\hat{H}_{n+1...N}$. Furthermore, the last term yields $(N-n)$ identical terms due to permutation symmetry of the wave function. We thus obtain

$$
\begin{aligned}
i\partial_t\Gamma^{(n)} = & (\hat{H}_{1...n} - \hat{H}_{1'...n'})\Gamma^{(n)} \\
& +\frac{N!}{(N-n-1)!}\sum_{i=1}^{n}\int d\mathbf{x}_{n+1}\Big([U(\mathbf{x}_i\mathbf{x}_{n+1}) - U(\mathbf{x}_i'\mathbf{x}_{n+1})] \\
& \Phi(X_n, \breve{X}_n, t)\Phi^*(X_n', \breve{X}_n, t)\Big). \quad (1.27)
\end{aligned}
$$

Using the definition of $\Gamma^{(n+1)}$ we can rewrite this as

$$
(i\,\partial_t - \hat{H}_{1...n} + \hat{H}_{1'...n'})\,\Gamma^{(n)}(X_n, X_n', t) = \\
\sum_{i=1}^{n}\int d\mathbf{x}_{n+1}(U(\mathbf{x}_i\mathbf{x}_{n+1}) - U(\mathbf{x}_i'\mathbf{x}_{n+1}))\Gamma^{(n+1)}(X_n\mathbf{x}_{n+1}, X_n'\mathbf{x}_{n+1}, t).
$$

$$(1.28)$$

As we can see from this equation, the equation of motion for each RDM contains the corresponding and one order higher RDM. The whole set of these interrelated equations form the so-called **BBGKY hierarchy** since a basically similar hierarchy was initially invented and developed

by Born, Bogoliubov, Green, Kirkwood and Yvon [26–29] in classical sta-
tistical mechanics. In fact, one can perform the Wigner transform on this
hierarchy to get the Wigner representation of it. Then, after some algebra
one can easily show that the classical limit of this hierarchy, i.e. $\hbar \to 0$, re-
duces to the classical BBGKY hierarchy, as it should. These calculations
have been performed in detail in Sec. 2.3.2 in Ref. [30].

However, it would not be practical to propagate the highest order of
the hierarchy and in order to propagate the lower order equations, we
need to truncate them. There are many theories in which the hierarchy
is truncated at the level of the first equation by approximating $\Gamma^{(2)}$ as a
functional of $\Gamma^{(1)}$; but in this thesis we will truncate the hierarchy at the
second level. The methods of the truncation and detailed discussion of the
results are presented in Chapter 3.

2. Electrons on the move

In this chapter, first, we provide a short introduction to the concept of electronic transport in mesoscopic systems where the conductor does not show Ohmic behavior and quantum mechanical effects start to play a role in the transport properties of the system. We also introduce the Landauer formula as a widely used method to calculate the conductivity in such systems.

Next, we apply this method to study the electronic transport in different nanoscale systems containing carbon nanotubes.

2.1 Landauer approach to electronic transport

If size of the conducting medium gets smaller than the phase-relaxation or coherent length of the system, we enter the *coherent regime* of electronic transport where the probability of phase destroying, inelastic scattering, *e.g.* by phonons, is negligible. Electronic transport through mesoscopic systems, like carbon nanotube based systems particularly at low temperatures, are categorized in this regime.

The most popular approach to the electronic transport in mesoscopic systems is the Landauer approach which relates the conductance of a sample
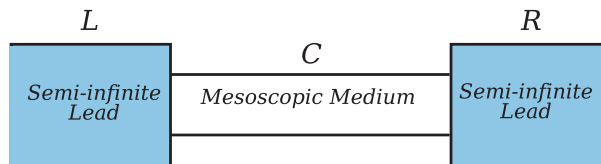

Figure 2.1. Schematic view of the ideal system used in Landauer formalism. A central mesoscopic medium (C), between two semi-infinite reflectionless leads in its left (L) and right (R).

to transmission probabilities of propagating electrons at the Fermi level. Consider a conducting sample (C), which is attached to two reflectionless leads, say left lead (L), and right lead (R) as depicted in Fig. 2.1. Further we assume that each lead has many scattering states (sometimes called propagating modes or channels) from which we choose N state with N being a large enough cut-off value. Then the Landauer formula for the conductance reads,

$$G(\varepsilon) = \frac{2e^2}{h} \sum_{n=1}^{N} T_n(\varepsilon), \qquad (2.1)$$

where ε is the energy and T_n is the transmission probability for the scattering state n, and is defined as $T_n = (t^{\dagger}t)_{nn}$. Here, t is the transmission matrix which its element $t_{nn'}$ is the probability that an incoming wave from the state n' in the left lead transmits into the state n in the right lead.

Conceptually, the Landauer formula suggests that the ballistic conductance is quantized in $2e^2/h$ units, but it only can be seen clearly if the transmission probability is either 0 or 1. For example, armchair single wall nanotubes have two different channels at the Fermi level which are fully open (transmission probability of 1) and therefore the conductance is $4e^2/h$. Reference [31] provides the derivation of Landauer formula with a detailed discussion on the subject of transport in mesoscopic systems.

A standard way to implement the Landauer approach is to express the scattering matrix in terms of Green's function which is approximated by ground-state Kohn-Sham Green's function. This DFT-based transport approach is what we use in our calculations. However, one should be aware of the limitations of this method, in order to apply it correctly. First of all, the DFT-based formulation of the Landauer approach, make it vulnerable to the DFT limitations as well. For instance, the accuracy of the ground-state functionals is one of the issues of concern particularly since the current flow is a nonequilibrium phenomenon in nature. On the other hand, the Landauer formalism itself is based on some assumptions that limits its applicability; for example, it assumes electrons to be non-interacting and it neglects inelastic scattering, e.g., by phonons, that can have considerable effect in some systems specially at higher temperatures. All these deficiencies, and many more [32, 33], tell us to apply this method with open eyes. As an example, this single-electron-based Landauer approach tends to overestimate the conductance in many cases, or it is not able to capture some important many-body effects such as Coulomb blockade or Kondo effect.

More advanced transport formalisms, e.g., based on master equation or nonequilibrium Green's function (NEGF), were developed to overcome some of these problems. To treat the nonequilibrium situations more accurately, NEGF formalism was combined with the time-dependent DFT [34, 35] or GW formalism [36, 37] as well. However for finite bias calculations, where the leads have different electrochemical potential, we use DFT-based NEGF [38] formalism in the present dissertation.

2.2 Electronic transport in defective carbon nanotubes

Since their discovery [39], carbon nanotubes (CNT) have been subjected to exhaustive studies both theoretically and experimentally. They are also listed among the main candidates for post-CMOS (Complementary metal–oxide–semiconductor) nanoelectronic devices because of their high carrier mobility as well as their structural stability. The electronic, optical, and transport properties of CNTs depend strongly on their geometry, offering great versatility, but at the same time posing a huge challenge because of difficulties in growing and isolating CNT's of a predetermined type. Defects, impurities and imperfections, as an inevitable but not necessarily an unfavorable feature of a real-world nanotube, have also attracted intense attention [40], because they can modify the electronic properties of nanotubes to some extent, perhaps even in a controllable way.

Sidewall chemical functionalization is a way to control or affect the properties of CNTs in order to extend their area of application, and it is already a well-established branch of research [41–44]. However, the low reactivity of the sidewall of CNTs make their functionalization process difficult. On the other hand, defects and imperfections are an inevitable part of real life CNTs and they also might be a favorable point for the attachment of functional groups. Nevertheless, functionalization only will be useful if we can do it in a controllable manner, for instance, by controlling the density of the functional groups.

A possible good host for the functional groups has been introduced by the discovery of a hybrid carbon nanostructure, the carbon nanobud (CNB) [45] that consists of an imperfect fullerene covalently bonded to a single-wall carbon nanotube (SWCNT) (see Fig. 2.2). Carbon nanobuds open a new way of functionalizing CNTs, in particular, because of the high reac-
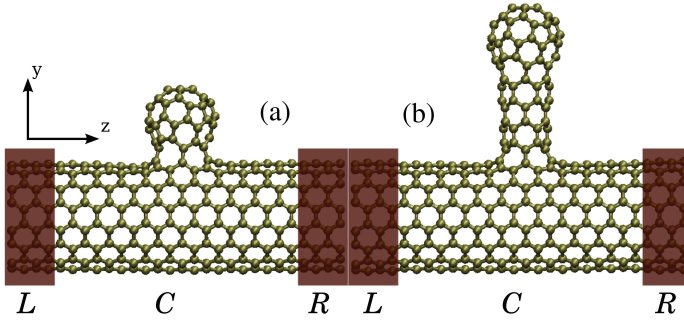
Figure 2.2. Typical carbon nanobud (CNB) structures studied in this work. The left leads (L), central regions (C) and, right leads (R) are shown in the figure. The CNB consists of an imperfect C60 attached to an armchair (8,8) single-wall carbon nanotube (SWCNT) via a neck region, made of a (6,0) SWCNT. The number of unit cells in the neck region can vary; panel (a) shows a zero-unit cell neck (CNB0), while (b) shows a two-unit cell neck (CNB2).

tivity of fullerenes [46, 47].

As one of the most important properties of the structure, we studied the electronic transport properties of CNBs in our first work [I].

Although the actual atomic structures of experimentally realized CNBs are not yet known, they can generally be categorized in two different groups, depending on how the fullerene is attached to the sidewall of the SWCNT [45, 48]. In the first type, a complete fullerene is covalently bonded to a SWCNT via sp^3-hybridization of carbon atoms e.g. [2+2] cycloaddition, while in the second type, all carbon atoms are sp^2-hybridized and the fullerene can be considered as a part of the SWCNT. In our work we focused on the second type of CNBs.

Based on the density-functional calculations of the structural stability reported in Ref. [45], we have chosen to model the CNB structures in the second group as follows (see Fig. 2.2). The dome of the CNB is an imperfect fullerene, C60, with six atoms removed at the apex. The fullerene is then attached to a (8,8) SWCNT via a connecting region ("neck") made of a varying number of unit cells of a (6,0) SWCNT. This construction allows a relatively smooth joining of the C60 to the underlying SWCNT, even though for the shortest neck regions the curvature for the connecting bonds is relatively high (see Fig. 2.2a). We use the notation CNBn, where n is the number of unit cells of the (6,0) SWCNT forming the neck, to describe the structures studied in this work.

As a general feature in all computed structures the transmission is reduced at the Fermi energy, E_f and above it. Moreover, there is a plateau region, with an almost perfect transmission, below the Fermi energy. Al-
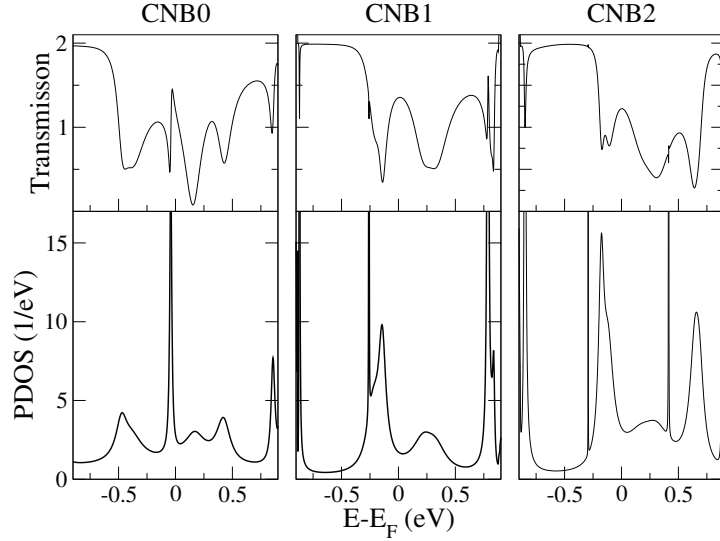
Figure 2.3. Transmission as a function of energy for nanobuds CNB0, CNB1, CNB2 (upper panels) and the PDOS for the bud and neck regions (lower panels).

though the details of these features differs, depending on the exact structure and the size of the neck, the overall features can be attributed to the vacancies in the structure and the localized states in the neck and bud regions.

The upper panel of Fig. 2.3, shows the transmission function for the CNB0-2 and the lower panel shows the projected density of state, PDOS, for the neck and bud regions. As it is shown, all of the dips in transmission have a direct correspondence with a peak in PDOS arising from the states that are (quasi)localized in the neck and bud regions. Also in the plateau
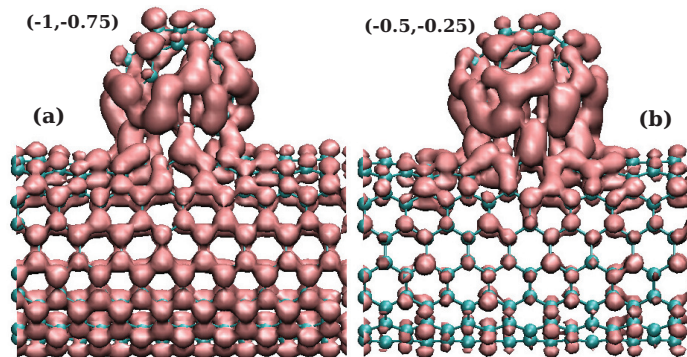

Figure 2.4. Local density of states, LDOS, of CNB0 for (a) the least perturbed energy window $(-1, -0.75)$ and (b) the most reduced energy window $(-0.5, -0.25)$.

part of the transmission, the bud and neck regions have a very low PDOS and the transmission is essentially the same as for a pristine SWCNT.

The effect of localized states in the neck and bud regions can be seen more clearly by calculating the local density of states, LDOS, which is spatial distribution of density of states (DOS) for a certain energy window. We calculated that LDOS for the CNB0 in two different energy windows; the almost unperturbed one, $(-1,-0.75)$, and the most reduced one, $(-0.5,-0.25)$, and they are both depicted in Fig. 2.4.

In the unperturbed window, DOS is distributed in the nanotube region of the CNB, as well as in the bud region (2.4a) and thus electrons transmit through the device as if the nanotube is perfect. On the other hand, in the most reduced energy window, the states are mostly localized in the bud region and they are distributed much less in the body of the CNB (2.4b) and hence in that energy window the transmission is almost suppressed.

Such analysis provides an insight for further manipulation of the CNB, e.g. gating it by chemical modification [49], in order to engineer nanodevices.

2.3   Effect of periodic bi-site perturbations

As continuation of the previous work, more studies were done on the effect of multiple buds on the electronic properties of CNTs, since the density of the buds can be modified experimentally. These studies have led us to the more general understanding of how periodic cluster perturbations, that include several neighboring carbon atoms in each cluster, affect the electronic structure of nanotubes. For example we performed calculations on different numbers of neighboring vacancies, hydrogen adsorbate clusters and nanobuds and the results showed the same pattern in all of them. Our next paper is devoted to explain that pattern. Hydrogen clusters are realistic defect candidates, because calculations and experiments show that adsorbed hydrogen atoms tend to cluster on SWCNTs' sidewalls [50–52] and hence we are demonstrating our analysis with these defect clusters.

Our detailed studies showed that [II], if the relative distance of perturbing clusters, i.e., bi-site defects which are extending over both A and B carbon sites, satisfies a certain condition, the metallic armchair SWCNT will turn semiconducting. We choose the (8,8) nanotube, on which four hydrogen atoms were adsorbed on neighboring carbon atoms, and we perform
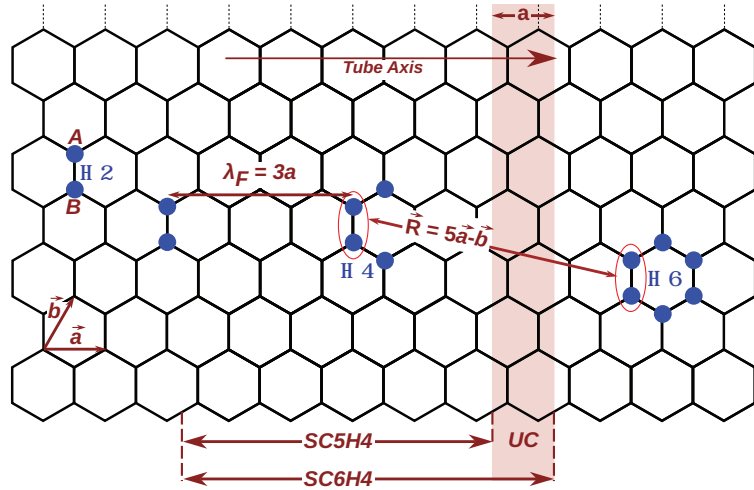
Figure 2.5. Three different hydrogen clusters -H2, H4 and H6 (blue circles)- used in the calculations. They are shown on a piece of an armchair SWCNT's surface. The unit vectors of the graphene sheet ($\vec{a}$ and $\vec{b}$), the A and B sublattices, the Fermi wavelength ($\lambda_F = 3a$), and a vector connecting the adjacent hydrogen clusters are also given. The unit cell (UC) of the pristine tube with the width "a", as well as superlattice unit cells corresponding to two different periodicity of the hydrogenated SWCNTs (SC5H4 and SC6H4) are shown.

band structure calculations for different supercell size of it. We adopt, for example, the notation SC5H4 for the supercell comprising five (8,8) SWCNT unit cells (SC5) and an adsorbed cluster of four hydrogen atoms (H4), as depicted in Fig.2.5. The essential criterion for these clusters is that they have to perturb both the A and B sublattices in a plane perpendicular to the tube axis.

Figure 2.6 shows the band structure for different supercell sizes, i.e., SC1H0, SC4H4, SC5H4, and SC6H4. Figure 2.6(a) depicts the band structure of the pristine single-unit-cell nanotube. Moreover, we know that multiplying the supercell length folds the band lines of the single-unit-cell nanotube. In Figs. 2.6(b)–2.6(d), the band structure of pristine nanotube for different supercell size is shown with dotted lines.

Nonetheless, the effect of H-clusters are different on different supercell sizes. For instance, in the cases of SC4H4 and SC5H4, the band lines are just slightly deviated from those of the pristine supercells of the same sizes, while for SC6H4, the differences are qualitative since a gap has been opened at the Fermi level and the metallic nanotube became semiconducting. The size of this gap increases with the strength of the perturbation. We found out that the gap opening only occurs for the supercell sizes in which the band crossing point at the Fermi energy falls near the
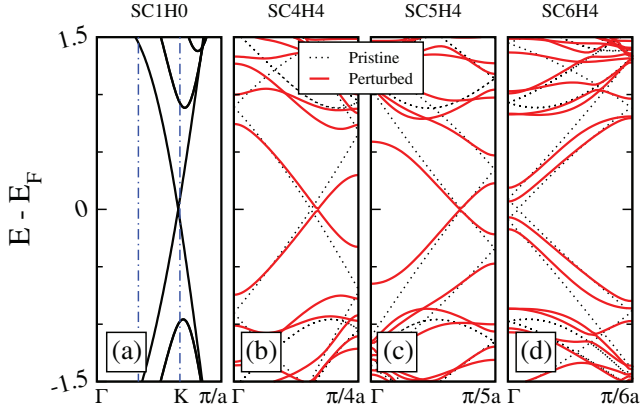
Figure 2.6. Effect of the periodically-repeated H4 clusters on the band structure of the (8,8) SWCNT. The band structure of (a) the pristine nanotube SC1H0 is compared to those for nanotubes with H-atom clusters and different supercell lengths, i.e., for (b) SC4H4, (c) SC5H4, and (d) SC6H4 (For the notation see the text and Fig. 2.5). "a" - on the wave vector axis - is the width of CNT unit cell as shown in Fig. 2.5. The dotted lines in (b) - (d) denote the band structure of the pristine nanotube folded according to the length of the supercell.

Γ point. With a simple band folding argument we can predict when this is happening; The (blue) dashed lines in Fig. 2.6(a) are band or Brillouin zone folding lines for SC3H0. similarly, for any SC(3M) with an integer M, these lines are two of the $3M - 1$ folding lines. Therefore in all these cases, the Fermi point is placed, after the folding, near the Γ-point.

More general calculations with supercells containing several H-atom clusters show that such a band gap opening happens for all supercells in which the relative positions of the adjacent adsorbate clusters, or more generally bi-site perturbations, fulfill the condition

$$\vec{R} = p\vec{a} + q\vec{b}, \qquad p - q = 3M, \qquad |M \in \mathbb{Z}, \qquad (2.2)$$

where $\vec{a}$ and $\vec{b}$ are the unit vectors given in Fig. 2.5.

To investigate the role of relative distance of the H-clusters more, we calculated the transmission function of several nanotubes with a varying number of perturbed supercells in the central region. For these calculations we employed a simple nearest neighbor tight-binding methods which is bench marked against the DFT results. The upper and lower panels of Fig. 2.7 show the transmission functions for the N(SC5H4) and N(SC6H4) central region systems, respectively, where N stands for number of periodically repeated H-clusters in the central region.

As it is clear, for SC5H4 cases (upper panels) the transmission around the Fermi energy remains very close to that of the pristine armchair SWCNT even when the number of scatterers increases. In contrast, in
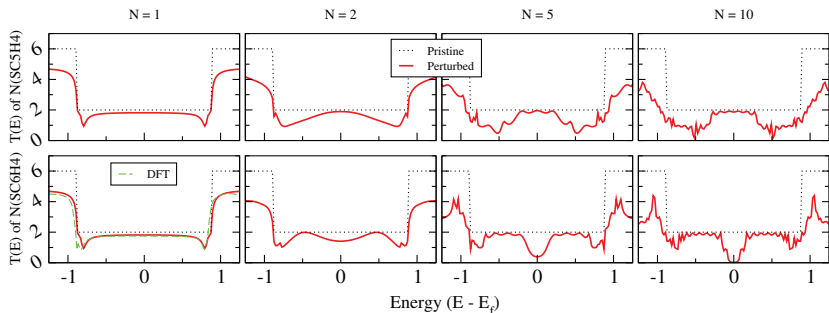
Figure 2.7. Effect of the relative positions and the number of bi-site perturbations on the transmission coefficient of armchair SWCNTs. The (red) solid curves in the upper and lower rows show the tight-binding results for central regions N(SC5H4) and N(SC6H4), respectively. From left to right, N=1, 2, 5 and 10. The dotted black lines give the pristine transmission function. The dashed (green) curve in the lower left panel gives the DFT result calculated by the TRANSIESTA program.

the case of SC6H4, multiple scatterers have a suppressive effect on the Fermi energy transmission so that the transmission drops nearly exponentially to zero with the number of scatterers. The rate of the decay depends on the strength of the scatterers [II].

Such a dependence on the relative distance can be described as follows. When the periodic perturbations occur with the separation of $n\,\lambda_F/2$, where n is an integer, all the backscattered electron waves at the Fermi level interfere constructively suppressing the transmission. As depicted in Fig. 2.5 the Fermi wavelength of an armchair SWCNT is $3a$ and therefore, the constructive interference of the backscattering waves takes place for periodic central regions constructed, for example, from the SC6H4 supercells but not for those containing, for example, SC5H4 supercells (See Fig. 2.5).

It is worth mentioning that the qualitative feature of this phenomenon is generally valid regardless of the type of perturbations and their position around the circumference perpendicular to the tube axis.

2.4 Intertube transport and formation of Schottky barrier

What we have been discussing so far, concerned with the effects of defects, imperfections, add atoms, and manipulated structures on the transport through single tubes. However, in real life devices, we also deal with bundles or networks of nanotubes. In order to understand the behavior of a CNT network or bundle, it is essential to capture the properties of the

junctions between nanotubes. In our third paper [III] we center our attention on crossed nanotube junctions and report the formation of Schottky barrier in special cases.

Typically, in production of CNTs their chiralities are distributed randomly, so that one third of the tubes are metallic, while the rest are semiconducting [53]. This leads to three different types of *intertube* (between two tubes) junctions, metallic-metallic (MM), semiconducting-semiconducting (SS) and metallic-semiconducting (MS).

In the CNT literature, ranging from experimental to *ab-initio* studies, many papers concentrate on carbon nanotube junctions (CNJs), especially on electron transport and conductance properties between two tubes [54–62]. Experiments show a finite junction resistance for the single wall nanotubes between 100 kΩ and 32 MΩ [57–59]. The numerical studies using density functional theory, and tight-binding (TB) methods give similar junction resistances, depending on the applied surface pressure over the junction [60]. The theory also predicts that the tunneling current depends strongly on the relative positions of atoms at the junction region [61] as well as on the angle between the crossed nanotubes [62].

In our paper, we present electronic transport properties of the MM, SS, and MS crossed junctions of single wall carbon nanotubes based on density functional theory with van der Waals (vdW) interactions included [63]. In addition, effect of n- and p-type doping, which can be thought to simulate the effect of a gate voltage, on the intertube transmission have been studied. It is shown that an MS junction forms a Schottky contact in the junction area, and a depletion region plays a dominant role at a particular doping. Moreover, we show the formation of deep bonding states between carbon atoms in different tubes. This causes charge accumulation in the junction area and has a considerable effect when the tubes are under pressure. This is called here, *the bonding charge effect*.

Two CNTs are set to form a crossed junction, as shown in the insets of figure 2.8. We choose nanotubes with (8,8) and (14,0) chiralities for metallic and semiconducting tubes, respectively. In order to perform transport calculations, the supercell has to be large enough for the four ends of the tubes to be close to the bulk structure. Therefore, we include 12 unit cells of armchair nanotubes and eight unit cells of zigzag nanotubes in the supercell. The distance between the nanotubes is defined by

$$d_c = d_{tc} - r_{t1} - r_{t2}, \tag{2.3}$$

where d_{tc} is the distance between the centers of mass of fixed atoms of the
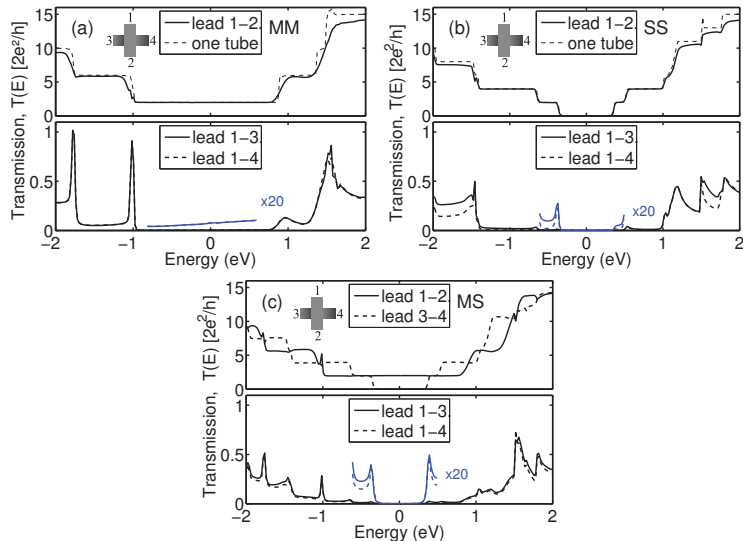
Figure 2.8. Intratube (upper panels) and intertube (lower panels) transmission functions $T(E)$ for (a) MM, (b) SS, and (c) MS junctions. The tubes are at their relaxed minimum energy distance from each other with the van der Waals correction. The values of the intertube transmissions near the Fermi level are plotted in on a larger scale for improved visibility. In (c) the leads 1 and 2 belong to the metallic tube, and the leads 3 and 4 to the semiconducting tube.

tubes and r_{t1} and r_{t2} are the radii of the nanotubes. Figure 2.8 shows the intratube and intertube transmission probabilities across different CNJs at the minimum energy configurations in the upper and lower panels respectively. The intratube transmission in the upper panels are very close to the one of pristine nanotubes and the small deformation of the tubes did not have a considerable effect on them.

The intertube transmissions are shown in the lower panels and they are magnified at the energies close the Fermi level. One can see that there is a slight transmission in the case of MM junction and no transmission for SS and MS junctions close to the Fermi level. These transmission gaps around the Fermi level can be attributed to the existing gap in the semiconducting tubes. Therefore, in order to get a nonzero transmission at the small bias limit, the nanotube needs to be doped or a gate voltage must be applied. We studied the effect of doping/gate voltage by adding extra positive or negative charges to the system, which are then compensated by a uniform background charge.

The intertube conductance of different CNJs at their Fermi level are shown in Fig. 2.9 for different doping ratios. The MM junction conductance stays approximately constant for all doping ratios in agreement with experiments [58]. In contrast, the SS junction shows a small and
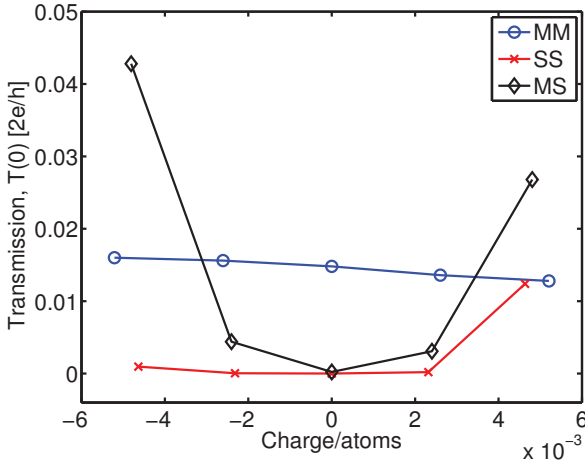
21

Figure 2.9. Intertube transmission of MM, SS, and MS junctions at Fermi level for different doping ratios. The tubes are at their relaxed minimum energy distance with the van der Waals correction.

highly asymmetrical behavior for positively and negatively doped structures. This behavior can be linked to the intertube transmission for the neutral case in Fig. 2.8(b), where the peaks close to 0.25 eV and -0.25 eV are not equal size.

As an important phenomenon, in addition to the potential barrier between the nanotubes, a Schottky barrier is formed in the MS junction originating from the different work functions of the doped tubes. The barrier can be seen in Fig. 2.10 where the charge distributions of the tubes are illustrated. In the junction area, the charge is transferred from the semiconducting to the metallic tube and a depletion region is formed. We define the depletion region as the area where the atoms have an opposite charge compared to the initially doped charge. In these calculations the size dependence of the depletion region on the doping ratio is not as strong as in an earlier work with a single nanotube and a Schottky barrier [64]. On the other hand, also here the depletion region shrinks fast with increasing doping ratio. The region size is 5 Å for $2 \cdot 10^{-3}$ e/atom doping ratio and it has already vanished for $4 \cdot 10^{-3}$ e/atom of both positive and negative doping ratios.

Besides the depletion region one can see a negative charge accumulation on a few atoms which have the shortest distance to the atoms in the other tube (pointed by arrows in Fig. 2.10). The amount of this extra charge is practically independent of the doping ratio. Our explanation for this charge accumulation follows. When the intertube distance becomes shorter, the p_z orbitals of those carbon atoms, which are close
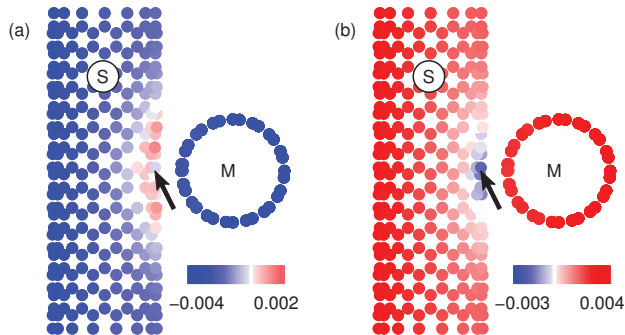
Figure 2.10. The Hirshfeld charges [65] for the MS junction with (a) negative and (b) positive doping ratios of $2 \cdot 10^{-3} e$/atom at the minimum energy geometries. The semiconducting tube shows a charge depletion region close to the junction. A local negative charge (pointed with an arrow) is visible as a blue atom inside a positively charged (red) depletion region (a) and as a darker blue atom in the negatively charged depletion region (b).

enough across the junction, start to overlap and form a weak bond with accumulating charges; these are what we referred as *bonding charges*.

In the paper [III] we showed that the bonding charge effect is much more pronounced in the CNJs under pressure when atoms are getting closer over the junction. The bonding states have also been seen by others [66] as states close to the energy gap of the semiconducting tube. However, the bonding charges do not contribute to the conductance since they are trapped at energies below the Fermi level.

While the bonding charges affect all the junctions MM, SS, and MS, the conductance behavior of an MS junction is affected also the Schottky depletion region: in the case of negative doping, when the depletion region is positively charged (Fig. 2.10(a)) , the bonding charges increase the size of the depletion region by pulling the electrons from nearby atoms, while concurrently the positive depletion region reduces the potential wall caused by the negative bonding charge. On the other hand, in the case of positively charged CNJs, the depletion region is negatively charged (Fig. 2.10(b)), and thus while the bonding charges reduce the depletion region they also increase the tunneling barrier. These effects describe the asymmetric transmission for the doped MS junction.

More detailed studies are performed in our paper [III] on the CNJs under pressure. That can mimic the real experimental environment and the effect of bending of nanotube networks on the transmission of single CNJ. We conclude that there are many phenomena that influence the transmission in CNJs and sometimes it becomes very complicated to explain their

effects separately.

All in all, in this chapter we provided a review of what we have done in the area of electronic transport in defective nanotubes and nanotube junctions. Moreover we explained how some of these studies might be used in engineering different electronic nanodevices. The next chapter will be attributed to the method development part of the thesis.

3. Truncation of BBGKY hierarchy

In Sec. 1.2.2 we described how the equation of motion for reduced density matrices led to a hierarchy or equation that is called BBGKY hierarchy. We also mentioned that in order to make the hierarchy practical, we must truncate it at some level, n, by reconstructing the $\Gamma^{(n+1)}$ as a functional of lower-order RDMs. For instance, if one approximates two-body RDM in terms of one-body RDM in the first equation, one arrives at the time-dependent version of reduced density matrix functional theory (TD-RDMFT). Similar to the TDDFT, most of the approximations used in TD-RDMFT are adiabatic extensions of the existing ground-state ones [7–9]; and even though they can successfully describe the ground state of some strongly correlated systems, they suffer from flaws such as lack of memory and time independent occupation numbers [67]. Furthermore, majority of these approximations do not necessarily conserve total energy of a system.

Some of these deficiencies will be cured if we consider propagating the first two equations of the hierarchy by approximating the three-body RDM. This is also useful since $\Gamma^{(1)}$ and $\Gamma^{(2)}$ are sufficient to calculate the dynamics of all one- and two-body observables. However, this prove to be a nontrivial task and in fact there are earlier attempts in nuclear dynamics [68, 69] which show that the fermionic inequality has been violated, indicating the non-fermionic nature of the corresponding RDM. Such behaviors were unexpected and it was claimed to be related to the violation of the relations between different orders of reduced density matrices, namely, the partial trace relation.

In this part of the thesis and in the paper [IV], we study the performance of such an approach for different truncation schemes in detail and show that the truncated set of equations may lead to instability and in many cases even divergence (in electronic density, occupation numbers, etc.). We mention the specific properties of approximations that are responsible

for these unphysical results. We will show that lack of properties such as positive-semidefiniteness also plays a crucial role in this failure. In addition, this study prompts one to be aware of the same issues which may arise in building approximations in TD-RDMFT.

3.1 Propagation methods and truncation scheme

As we mentioned, here we will only propagate $\Gamma^{(1)}$ and $\Gamma^{(2)}$ and therefore the first two equations of the hierarchy. The explicit form of these two equations are

$$(i\,\partial_t - \hat{h}_1 + \hat{h}_{1'})\,\gamma(\mathbf{x}_1, \mathbf{x}_1', t) = \int d\mathbf{x}_2\,(U(\mathbf{x}_1\mathbf{x}_2) - U(\mathbf{x}_1'\mathbf{x}_2))\Gamma(\mathbf{x}_1\mathbf{x}_2, \mathbf{x}_1'\mathbf{x}_2, t) \quad (3.1)$$

and

$$(i\,\partial_t - \hat{H}_{12} + \hat{H}_{1'2'})\,\Gamma(\mathbf{x}_1\mathbf{x}_2, \mathbf{x}_1'\mathbf{x}_2', t) =$$
$$\int d\mathbf{x}_3\,(U(\mathbf{x}_1\mathbf{x}_3) + U(\mathbf{x}_2\mathbf{x}_3) - U(\mathbf{x}_1'\mathbf{x}_3) - U(\mathbf{x}_2'\mathbf{x}_3))\Gamma^{(3)}(\mathbf{x}_1\mathbf{x}_2\mathbf{x}_3, \mathbf{x}_1'\mathbf{x}_2'\mathbf{x}_3, t),$$
$$(3.2)$$

where, here and throughout the rest of the text, $\gamma \equiv \Gamma^{(1)}$ and $\Gamma \equiv \Gamma^{(2)}$. As is customary in the literature [30], we call the right-hand side of Eq. (3.2) the three-body collision integral and use S to refer to it.

At this point we highlight an important property of the BBGKY hierarchy and the effect of truncation on it. As a direct outcome of Eq. (1.20), different levels of the hierarchy are compatible; namely, equations in the higher levels of the hierarchy are reducible to the lower-level ones. We refer to this link between equations as *compatibility* condition that preferably should be fulfilled by a good approximation. Thus, compatibility signifies that the highest equation is equivalent to the whole BBGKY hierarchy. This is not surprising since the highest equation is basically the original Schrödinger equation. However, when we truncate the hierarchy by introducing an approximation for $\Gamma^{(3)}$, the partial trace relation between $\Gamma^{(3)}$ and Γ does not necessarily hold and thus it generally breaks the compatibility between Eqs. (3.1) and (3.2). Consequently, when we truncate the BBGKY hierarchy, we have two generally distinct options to propagate the equations which should be equivalent if the truncation approximation satisfies compatibility.

1. *Propagating two coupled equations*. We can evolve both γ and Γ by solving Eqs. (3.1) and (3.2) together as coupled equations since the two

equations most likely are not compatible anymore after approximating $\Gamma^{(3)}$ in Eq. (3.2).

2. *Propagating only the second equation.* To avoid the problem of compatibility between two equations, we can evolve only Eq. (3.2). Then we assign γ to be the partial trace of Γ and denote it as γ_Γ to distinguish it from general γ. It mathematically reads

$$\gamma_\Gamma(\mathbf{x}_1, \mathbf{x}_1', t) = \frac{1}{N-1} \int d\mathbf{x}_2 \, \Gamma(\mathbf{x}_1\mathbf{x}_2, \mathbf{x}_1'\mathbf{x}_2, t). \tag{3.3}$$

In this way, we prevent the complication of dealing with two coupled equations.

In the paper [IV], we rigorously showed that regardless of the approximations we use, the first approach always keeps the total energy of the system conserved, while this happens only for some of the approximations in the second approach, Therefore, in general the first approach is preferred.

Now, we are ready to truncate the Eq. (3.2) by approximating $\Gamma^{(3)}$ in terms of γ and Γ. One systematic way of building these approximations is called *cluster expansion* which is a method of reconstructing higher-order RDMs as anti-symmetrized products of lower-order ones plus a residual correlation function [70–74]. To have a compact notation, first we define the wedge product as the anti-symmetrized product of p- and m-point functions by

$$a(X_p, X_p') \wedge b(\check{X}_p, \check{X}_p') = \tag{3.4}$$
$$\left(\frac{1}{N!}\right)^2 \sum_{\alpha,\beta} \epsilon(\alpha) \, \epsilon(\beta) \, a(\mathbf{x}_{\alpha_1} \ldots \mathbf{x}_{\alpha_p}, \mathbf{x}_{\beta_1}' \ldots \mathbf{x}_{\beta_p}') \, b(\mathbf{x}_{\alpha_{p+1}} \ldots \mathbf{x}_{\alpha_N}, \mathbf{x}_{\beta_{p+1}}' \ldots \mathbf{x}_{\beta_N}').$$

Here, $N = p + m$, α represents all permutations of the unprimed coordinates, β represents all permutations of the primed ones, and the function $\epsilon(\alpha)$ returns $+1$ when the permutation α contains an even number of transpositions and -1 for an odd number of transpositions [75]. For instance, the wedge product of two general one-particle matrices is

$$a(\mathbf{x}_1, \mathbf{x}_1') \wedge b(\mathbf{x}_2, \mathbf{x}_2') = \frac{1}{4}\Big\{ a(\mathbf{x}_1, \mathbf{x}_1')b(\mathbf{x}_2, \mathbf{x}_2') - a(\mathbf{x}_1, \mathbf{x}_2')b(\mathbf{x}_2, \mathbf{x}_1') \tag{3.5}$$
$$+ a(\mathbf{x}_2, \mathbf{x}_2')b(\mathbf{x}_1, \mathbf{x}_1') - a(\mathbf{x}_2, \mathbf{x}_1')b(\mathbf{x}_1, \mathbf{x}_2') \Big\}.$$

Now, we illustrate the cluster expansion by some examples. The first term of the expansion of $\Gamma^{(n)}$ has the same form as in the noninteracting-particle picture, namely, it is an n-dimensional determinant of γ, with

$\gamma(\mathbf{x}_i, \mathbf{x}'_j, t)$ placed in row i and column j. For instance, for $\Gamma^{(2)}$, the first term reads

$$\begin{vmatrix} \gamma(\mathbf{x}_1, \mathbf{x}'_1, t) & \gamma(\mathbf{x}_1, \mathbf{x}'_2, t) \\ \gamma(\mathbf{x}_2, \mathbf{x}'_1, t) & \gamma(\mathbf{x}_2, \mathbf{x}'_2, t) \end{vmatrix} \equiv 2\,\gamma \wedge \gamma. \tag{3.6}$$

Now, we define a two-body correlation function, $\Delta^{(2)}$, as a means of the deviation of Γ from the noninteracting form such that

$$\Gamma(X_2, X'_2, t) = 2\,\gamma \wedge \gamma + \Delta^{(2)}(X_2, X'_2, t). \tag{3.7}$$

If we, for instance, approximate $\Gamma_{app} = 2\gamma \wedge \gamma$ and replace it in the first equation of the BBGKY hierarchy (3.1), we recover immediately the well-known TDHF equation.

For $\Gamma^{(3)}$ accordingly, we use a noninteracting particle form and add anti-symmetrized products of γ with the correlation function $\Delta^{(2)}$ – that partly describe the 3-body correlation – plus a remainder, $\Delta^{(3)}$, i.e.

$$\Gamma^{(3)}(X_3, X'_3, t) = \begin{vmatrix} \gamma(\mathbf{x}_1, \mathbf{x}'_1, t) & \gamma(\mathbf{x}_1, \mathbf{x}'_2, t) & \gamma(\mathbf{x}_1, \mathbf{x}'_3, t) \\ \gamma(\mathbf{x}_2, \mathbf{x}'_1, t) & \gamma(\mathbf{x}_2, \mathbf{x}'_2, t) & \gamma(\mathbf{x}_2, \mathbf{x}'_3, t) \\ \gamma(\mathbf{x}_3, \mathbf{x}'_1, t) & \gamma(\mathbf{x}_3, \mathbf{x}'_2, t) & \gamma(\mathbf{x}_3, \mathbf{x}'_3, t) \end{vmatrix} \tag{3.8}$$
$$+ \sum_{i,j=1}^{3} (-1)^{i+j} \gamma(\mathbf{x}_i, \mathbf{x}'_j, t) \Delta^{(2)}(\check{\mathbf{x}}_i, \check{\mathbf{x}}'_j, t) + \Delta^{(3)}(X_3, X'_3, t).$$

In the second term on the right-hand side, $\check{\mathbf{x}}_j$ denotes the pair of variables in the set $(\mathbf{x}_1\mathbf{x}_2\mathbf{x}_3)$ complementary to $\mathbf{x}_j$ keeping the order of the arguments fixed; the same goes for the primed coordinates. For example, $\check{\mathbf{x}}_2 = (\mathbf{x}_1\mathbf{x}_3)$. Using the wedge product notation, we can rewrite Eq. (3.8) as

$$\Gamma^{(3)} = 6\,\gamma \wedge \gamma \wedge \gamma + 9\,\gamma \wedge \Delta^{(2)} + \Delta^{(3)} = -12\,\gamma \wedge \gamma \wedge \gamma + 9\,\gamma \wedge \Gamma + \Delta^{(3)} \tag{3.9}$$

in which we replaced the $\Delta^{(2)} = \Gamma - 2\,\gamma \wedge \gamma$ from Eq. (3.7). Similarly, we can write the expansion for higher-order RDMs.

The same method has been used in the Contracted Schrödinger Equation formalism (the hierarchical set of equations for density matrices derived from the time independent Schrödinger equation) and referred to as *cumulant expansion* [76–79]. Nakatsuji and Yasuda made the expansion more grounded by deriving it using the relation between RDMs and Green's functions [77]. Based on these, we are now ready to discuss a number of approximations for $\Gamma^{(3)}$:

1. *Three-body collision-integral-free (3b-CIF) approximation.* The simplest one rises from the assumption of $\Gamma^{(3)} = 0$, which removes the whole right-hand-side of Eq. (3.1).

2. *Three-body-noninteracting approximation (3b-NIA).* This is obtained only by considering the noninteracting term of Eq. (3.9)

$$\Gamma_{3b-NIA}^{(3)} = 6\,\gamma \wedge \gamma \wedge \gamma. \tag{3.10}$$

This gives $\Gamma^{(3)}$ as a functional of γ.

3. *WC approximation.* We can, of course, climb to the next level and take also the second term of Eq. (3.9) into account which leads us to

$$\Gamma_{WC}^{(3)} = -12\,\gamma \wedge \gamma \wedge \gamma + 9\,\gamma \wedge \Gamma, \tag{3.11}$$

where the index stands for Wang and Cassing who introduced this approximation in 1985 [70]. This properly reduces to Eq. (3.10) when we assume $\Gamma = 2\gamma \wedge \gamma$.

Although these are the main approximations that we study, they are not the only ones. Some other approximations have been used in the paper for analysis purposes and a list of more approximations is provided in Tables 3.2 and 3.3.

3.2 Matrix representation of the equations

In order to implement and solve the equations, we need to represent them in a suitable basis set. Assuming an orthonormal basis set $\{\varphi_i\}$, we can rewrite the γ and Γ as

$$\gamma(\mathbf{x}, \mathbf{x}', t) = \sum_{ij} \gamma_{ij}(t)\,\varphi_i^*(\mathbf{x}')\varphi_j(\mathbf{x}) \tag{3.12}$$

$$\Gamma(\mathbf{x}_1\mathbf{x}_2; \mathbf{x}_1'\mathbf{x}_2', t) = \sum_{ijkl} \Gamma_{ijkl}(t)\,\varphi_i^*(\mathbf{x}_1')\varphi_j^*(\mathbf{x}_2')\varphi_k(\mathbf{x}_1)\varphi_l(\mathbf{x}_2) \tag{3.13}$$

and we will further define

$$h_{ij}(t) = \int \varphi_i^*(\mathbf{x}_1)\hat{h}(\mathbf{x}_1, t)\varphi_j(\mathbf{x}_1)\,d\mathbf{x}_1 \tag{3.14}$$

$$U_{ijkl} = \int \varphi_i^*(\mathbf{x}_1)\varphi_j^*(\mathbf{x}_2)U(\mathbf{x}_1\mathbf{x}_2)\varphi_k(\mathbf{x}_1)\varphi_l(\mathbf{x}_2)\,d\mathbf{x}_1 d\mathbf{x}_2, \tag{3.15}$$

where due to hermicity of the matrices we have

$$\begin{aligned} \gamma_{ji} &= \gamma_{ij}^* & \Gamma_{klij} &= \Gamma_{ijkl}^* \\ h_{ji} &= h_{ij}^* & U_{klij} &= U_{ijkl}^*. \end{aligned} \tag{3.16}$$

Also, the antisymmetry of $\Gamma(\mathbf{x}_1\mathbf{x}_2; \mathbf{x}_1'\mathbf{x}_2')$ leads to

$$\Gamma_{jikl} = \Gamma_{ijlk} = -\Gamma_{ijkl}. \tag{3.17}$$

Then, Eq. (3.1) reads

$$\sum_{kl} [i\partial_t \gamma_{kl}(t)] \, \varphi_k^*(\mathbf{x}_1')\varphi_l(\mathbf{x}_1) = \sum_{kl} \gamma_{kl}(t) \, [\hat{h}(\mathbf{x}_1,t) - \hat{h}(\mathbf{x}_1',t)]\varphi_k^*(\mathbf{x}_1')\varphi_l(\mathbf{x}_1)$$

$$+ \sum_{klmn} \Gamma_{klmn}(t) \left(\int \varphi_l^*(\mathbf{x}_2)[U(\mathbf{x}_1\mathbf{x}_2) - U(\mathbf{x}_1'\mathbf{x}_2)]\varphi_n(\mathbf{x}_2)\,d\mathbf{x}_2 \right) \varphi_k^*(\mathbf{x}_1')\varphi_m(\mathbf{x}_1).$$

$$(3.18)$$

Now we multiply this equation by $\varphi_i(\mathbf{x}_1')\varphi_j^*(\mathbf{x}_1)$ and integrate over $\mathbf{x}_1, \mathbf{x}_1'$ that results in

$$i\partial_t \gamma_{ij}(t) =$$

$$\sum_k \left[\gamma_{ik}(t)h_{jk}(t) - \gamma_{kj}(t)h_{ki}(t) \right] + \sum_{klm} \left[\Gamma_{iklm}(t)U_{jklm} - \Gamma_{kljm}(t)U_{klim} \right]. \quad (3.19)$$

For transforming the second equation (3.2) the same method can be applied where the final result depends on the employed approximation for $\Gamma^{(3)}$. For instance, for 3b-NIA approximation in Eq. (3.10), we arrive at

$$\begin{aligned}
i\partial_t \Gamma_{ijkl} &= \sum_m \big[\Gamma_{ijml}(t)h_{km}(t) + \Gamma_{ijkm}(t)h_{lm}(t) - \Gamma_{mjkl}(t)h_{mi}(t) \\
&\quad - \Gamma_{imkl}(t)h_{mj}(t) \big] + \sum_{rs} \left[\Gamma_{ijrs}(t)U_{klrs} - \Gamma_{rskl}(t)U_{rsij} \right] \qquad (3.20) \\
&\quad + \sum_{qrs} \big[\left(\gamma_{iq}(t)\gamma_{js}(t)\gamma_{rl}(t) - \gamma_{jl}(t)\gamma_{iq}(t)\gamma_{rs}(t) \right) (U_{krsq} - U_{krqs}) \big] \\
&\quad + \sum_{qrs} \big[\left(\gamma_{iq}(t)\gamma_{js}(t)\gamma_{rk}(t) - \gamma_{jk}(t)\gamma_{iq}(t)\gamma_{rs}(t) \right) (U_{lrqs} - U_{lrsq}) \big] \\
&\quad + \sum_{qrs} \big[\left(\gamma_{qk}(t)\gamma_{sl}(t)\gamma_{jr}(t) - \gamma_{jl}(t)\gamma_{qk}(t)\gamma_{sr}(t) \right) (U_{qsir} - U_{sqir}) \big] \\
&\quad + \sum_{qrs} \big[\left(\gamma_{qk}(t)\gamma_{sl}(t)\gamma_{ir}(t) - \gamma_{il}(t)\gamma_{qk}(t)\gamma_{sr}(t) \right) (U_{sqjr} - U_{qsjr}) \big] \\
&\quad + \sum_{qrs} \gamma_{rs}(t)\gamma_{jq}(t) \big[\gamma_{il}(t)(U_{rkqs} - U_{krqs}) + \gamma_{ik}(t)(U_{lrqs} - U_{rlqs}) \big] \\
&\quad + \sum_{qrs} \gamma_{sr}(t)\gamma_{ql}(t) \big[\gamma_{jk}(t)(U_{qsir} - U_{qsri}) + \gamma_{ik}(t)(U_{qsrj} - U_{qsjr}) \big].
\end{aligned}$$

In the case of spin compensated systems, there are many symmetries that simplify the equations further and increase efficiency of the calculations.

3.3 Test model implementation

Now, we have to choose a model system which is appropriate for testing different approximations. The linear-chain Hubbard model fits very well here since first of all we can solve it exactly for a few sites; and secondly, since the number of single-particle orbitals that build the many-body Hilbert space is limited, we can retain the full single-particle basis set and avoid basis-set truncation errors.

On the other hand, to study the quality of the approximations, we must go beyond two-particle systems since they can be treated exactly in our formalism. Thus, we will avoid the practical complications introduced by spin in odd-number-electron systems (that does not affect the generality of our results), and perform all our calculations in a four-site Hubbard chain with four electrons and without periodic boundary conditions. There, we only consider the nearest neighbor hopping and on-site Coulomb interaction, and then the Hubbard Hamiltonian in second quantization notation reads

$$\hat{H} = \sum_{\sigma, i} t \, (a_{i+1,\sigma}^{\dagger} a_{i,\sigma} + a_{i,\sigma}^{\dagger} a_{i+1,\sigma}) + \sum_{i} U \, n_{i\uparrow} n_{i\downarrow}, \qquad (3.21)$$

where σ is a spin index, i is the site index and t and U denote hopping and on-site Coulomb potential energy, respectively. Here, t is set to unity and U gets different values to simulate different correlation strengths.

In our code, we only propagate the lower triangular part of γ and Γ since they should be Hermitian matrices. For solving the differential equations, we use the fourth-order Runge-Kutta method. However, to ensure the accuracy and stability of our results, we also implemented more accurate time-propagation schemes such as the fourth-order Adams-Bashforth-Moulton method (for a detailed discussion of these methods see [80]). We also performed many tests, with γ, Γ and $\Gamma^{(3)}$ extracted and replaced from the exact calculations, to guarantee a flawless implementation.

3.4   Results and discussion

In this part, we mainly investigate three different approximations of $\Gamma^{(3)}$, namely the three-body collision integral free, the three-body non-interacting, and the WC approximations and compare them with the exact and the TDHF results. With these approximations, we have now a closed set of equations and as for any differential equation, we need an initial state of the system to propagate them. To study the initial state dependence of the phenomena, we choose two extreme regimes of initial states to perform our calculations: far from equilibrium and close to equilibrium.

At first, we choose a far from equilibrium state as our initial state since it helps us to show the problem more clearly. We build such an initial state by putting four electrons in the two leftmost sites, i.e.

$$|\Psi_0\rangle = a_{1,\uparrow}^{\dagger} a_{1,\downarrow}^{\dagger} a_{2,\uparrow}^{\dagger} a_{2,\downarrow}^{\dagger} |0\rangle, \qquad (3.22)$$
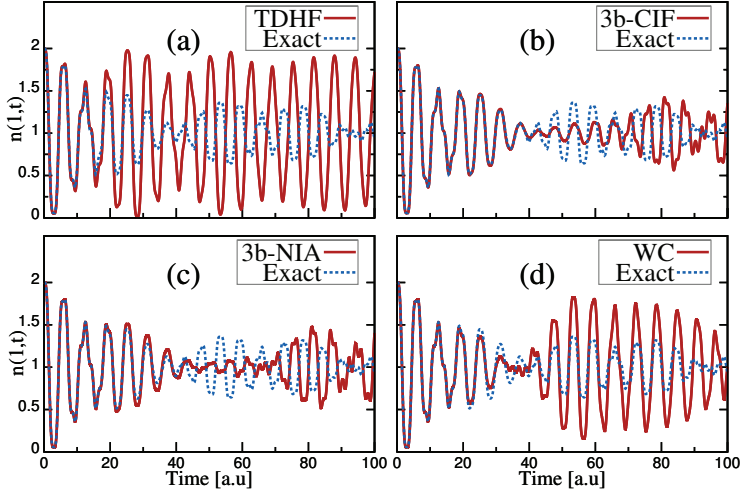
Figure 3.1. Time evolution of electronic density in the leftmost site of a 4-site Hubbard model with (a) TDHF (b) 3b-CIF (c) 3b-NIA and, (d) WC approximations. The exact result is also given for comparison. Here, m, $\hbar$ are set to unity and Hubbard parameters are $U = 0.1$ and $t = 1$. The four electrons filled the two leftmost sites initially.

where 1 and 2 refer to two neighboring sites at the beginning of the chain. Here, since this initial state is a Slater determinant formed by two site-orbitals, Γ has the exact form of Eq. (3.6), but this is not the case for all the initial states. The time evolution of electronic density in the leftmost site, n(1,t), is plotted in Fig. 3.1 for a weak on-site Coulomb energy, $U = 0.1$, and for (a) TDHF, (b) 3b-CIF, (c) 3b-NIA and, (d) WC approximation. The plots also contain the exact result for comparison. In a short-time scale, we can see that all three approximations improve the quality of the results considerably, compared to the TDHF. However, comparing with each other, the approximations do not exhibit large differences.

Figure 3.2 shows the time evolution of the highest and lowest natural orbital occupation numbers. For TDHF, as in many other TD-DMFT approximations, the occupation numbers are time independent, which is a challenge in that community as we mentioned [67]. Here, we can see that the WC approximation, despite its amplitude, follows the trend of the exact result more closely as one might expect.

Surprises show up when we propagate the equations further. Figure 3.3 shows essentially the same results as in 3.1, for a longer propagation time. It also shows how the highest and lowest geminal occupation numbers, λ_{max} and λ_{min}, behave in time. For the 3b-CIF in panel (a) we can
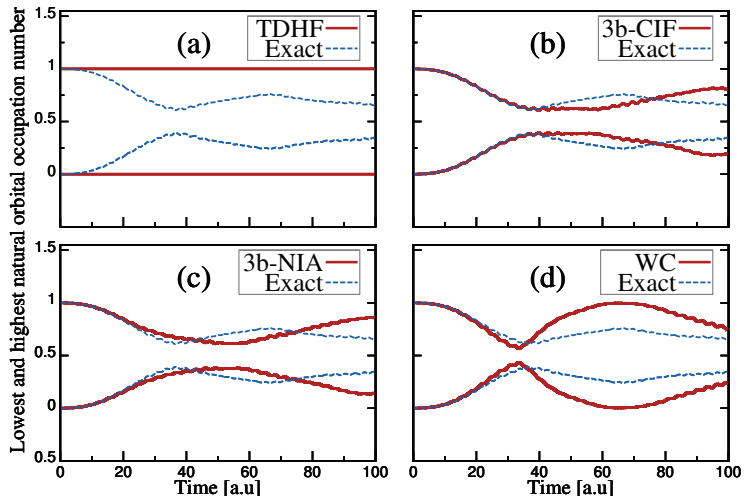
Figure 3.2. Highest and lowest natural orbital occupation number in a 4-site Hubbard model with (a) TDHF (b) 3b-CIF (c) 3b-NIA and, (d) WC approximations. The exact result is also given for comparison. Here, m, $\hbar$ are set to unity and Hubbard parameters are $U = 0.1$ and $t = 1$. The four electrons filled the two leftmost sites initially.

see unphysical behaviour around $t \approx 240\,a.u$, where the density acquires negative values or rises beyond two electrons in a site. The problem is more serious for the two other approximations since for longer propagation times, the electronic density starts to oscillate with amplitudes much beyond physically allowed boundaries, and eventually diverges as is shown in Fig. 3.3 (b and c). The divergence time depends on the correlation strength, namely on the value of U in our model, and it is inversely proportional to a power of U. For example, for WC approximation, the divergence time changes from $t \approx 532\,a.u$ for $U = 0.1$ to $t \approx 3.7\,a.u$ for $U = 5$. We depict the U-dependency of the divergence time, for WC approximation, in Fig. 3.4. It is important to note that in 3b-NIA and WC approximations, λ_{max} and λ_{min} start to diverge much earlier, although we can not immediately see the effect in neither natural orbital occupation numbers nor on-site electronic densities.

It is well-known that the time-evolution of a far from equilibrium state is generally very difficult to handle with any approximation, and particularly with the ground-state-tuned ones; hence, we change the initial states to be closer to the system's ground state in order to investigate the generality of this phenomenon. We start the simulation with the initial γ and Γ extracted from the ground state of i) the exact solution and ii) the
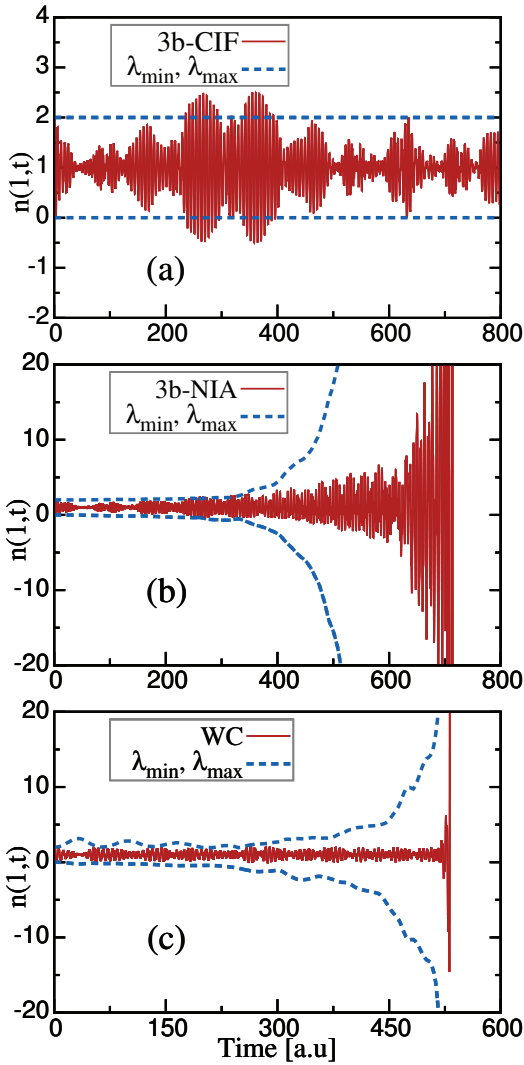
Figure 3.3. Time evolution of electronic density in the leftmost site of a 4-site Hubbard model in a longer time scale for (a) 3b-CIF (b) 3b-NIA, (c) WC approximations. Blue lines show the highest and lowest geminal occupation number in time. Here, m, $\hbar$ are set to unity and Hubbard parameters are $U = 0.1$ and $t = 1$. The four electrons filled the two leftmost sites initially.
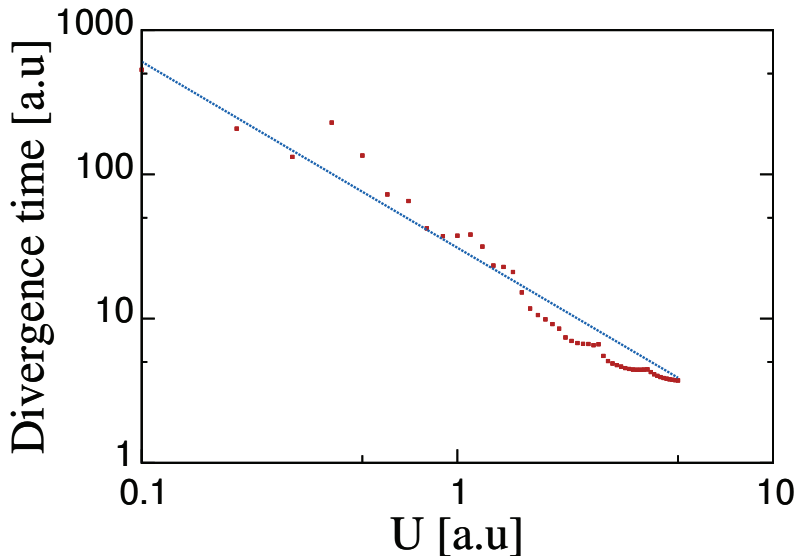
Figure 3.4. Divergence time of electronic density in a 4-site Hubbard model for WC approximation versus on-site Coulomb energy U (both in logarithmic scale). Blue line is the fitted line. Here, m, $\hbar$ are set to unity and Hubbard parameter $t = 1$. The four electrons filled the two leftmost sites initially.

Hartree-Fock approximation; and let it propagate with all three different approximations.

For the initial state being the ground state of HF, we again use the Eq. (3.6) to build the Γ from γ since this state is also made of a Slater determinant of two site-orbitals. In the case that we start from the exact ground state, we extract the exact γ and Γ and feed them into the equations.

Although in these cases the electronic density for the 3b-CIF does not violate physical bounds, we still see the divergence for other two approximations. Figure 3.5 shows the time propagation for the three mentioned approximation when the initial state is the ground state of Hartree-Fock approximation. In the case of WC approximation, the divergence occurs much later than the far from equilibrium initial state, while for 3b-NIA, it occurs a bit earlier. This shows that we cannot claim any particular dependence on the initial state in our models.

Moreover, we used the method introduced by Mazziotti [81] to find the ground state associated with 3b-NIA and WC approximations and then used it as the initial state. However, since the method [81] is not totally convergent, the result is not a truly stationary state and even starting from such state does not bring stability to the equations and divergence
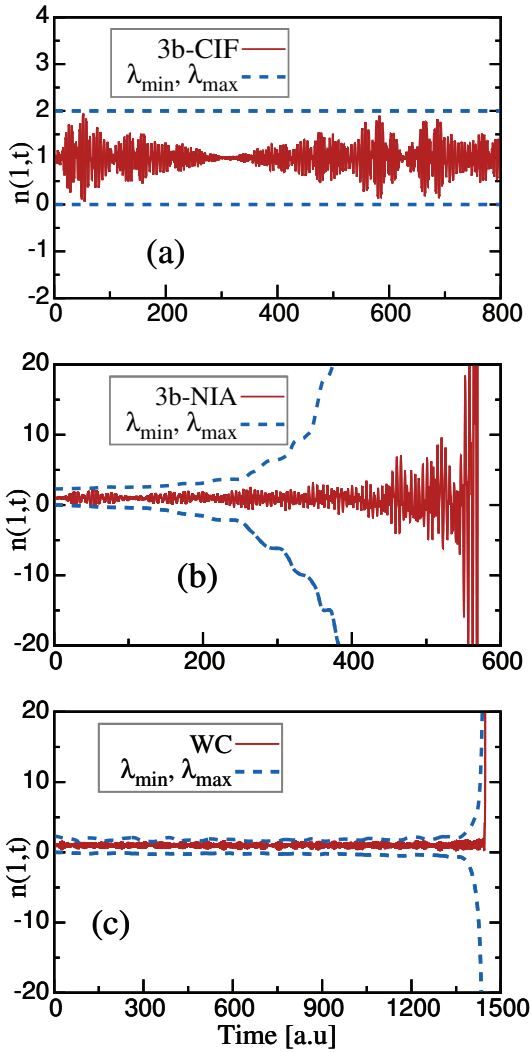
Figure 3.5. Time evolution of electronic density in the leftmost site of a 4-site Hubbard model (a) 3b-CIF (b) 3b-NIA, (c) WC approximations when we used the ground state of Hartree-Fock approximation as the initial state. Blue lines show the highest and lowest geminal occupation number in time. Here, m, $\hbar$ are set to unity and Hubbard parameters are $U = 0.1$ and $t = 1$.

appears again.

These tests show that the divergence problem is independent of the initial state and has to do with the nature of the approximated equations. It is worth emphasizing again that in all of these approximations the continuity condition has not been violated and the total number of particles is always conserved. Nevertheless, the continuity equation does not guarantee that the electronic density in each state does not go below zero or beyond two.

As we mentioned in the introduction, the violation of fermionic inequality has also been observed for a different system in nuclear physics [68, 69]. In fact, there are earlier works in the classical BBGKY theory in which they studied the effect of nonlinearity introduced by truncation of the hierarchy, and showed the existence of instability in these coupled equations depending on the initial conditions of the system [82, 83]. Other studies also indicated that the classical collision integral can diverge [84, 85]. Such catastrophic behaviors of these coupled equations pose a valid question that, why these highly advanced approximations based on the Green's function expansion fail to follow fundamental physical principles, and even lead to divergence, even though the total energy and number of particles are conserved.

The instability of the propagations is not limited to these two equations, and it can be seen even in TDHF where we only keep the first equation Eq. (3.1). Although it is known that TDHF never diverges, the nonlinearity introduced into the equation can give rise to chaotic and unphysical behaviors as Schmitt *et al.* showed in their work [86, 87]. We can illustrate such a unphysical behavior in the context of our four-particle in four-site Hubbard model when $U = 10$. We choose our initial RDM, γ_{init}, to be an ensemble of the ground state, γ_0, and the second excited state, γ_2, of Hartree-Fock. Namely,

$$\gamma_{init}(\mathbf{x}, \mathbf{x}') = (1 - \epsilon)\,\gamma_0(\mathbf{x}, \mathbf{x}') + \epsilon\,\gamma_2(\mathbf{x}, \mathbf{x}'), \qquad (3.23)$$

where ϵ is an infinitesimally small coefficient (10^{-12} in our calculation) which makes γ_{init} extremely close to γ_0. Using the time-dependent Schrödinger equation we can easily show that the combination of the ensemble should stay the same over the time, i.e,

$$\gamma_{init}(\mathbf{x}, \mathbf{x}', t) = (1 - \epsilon)\,\gamma_0(\mathbf{x}, \mathbf{x}', t) + \epsilon\,\gamma_2(\mathbf{x}, \mathbf{x}', t). \qquad (3.24)$$

Therefore, we expect the time evolution of the γ_{init} to stay nearly steady. However, as we show in Fig. 3.6, its TDHF propagation shows very large
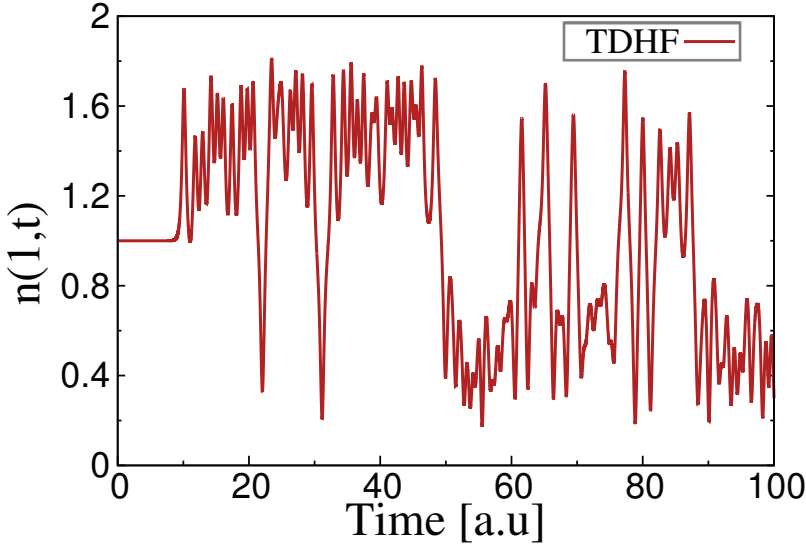
Figure 3.6. Emergence of chaotic behaviour in electronic density in the leftmost site of a 4-site Hubbard model for TDHF approximation. Here, m, $\hbar$ are set to unity and Hubbard parameters are $U = 10$ and $t = 1$. The initial $\gamma(0)$ is chosen from Eq. (3.23) with $\epsilon = 10^{-12}$.

irregular fluctuations which are characteristic for chaotic behaviors. This happens due to the nonlinearity that was introduced by approximation of Γ.

To analyze the divergent behavior of the equations, we center our attention to the basic properties of the BBGKY hierarchy and density matrices to find out how they are affected by different approximations. As we already showed, the employed approximations break the compatibility between Eq. (3.1) and the approximated version of Eq. (3.2) and the partial trace relation (Eq. (1.20)) between Γ and γ does not hold any more. Schmitt *et al.* [68] and Gherega *et al.* [69] claimed this to be the main source of the problem. On the other hand, it is obvious that the positive-semidefiniteness of density matrices has also been violated. This problem may arise for one of the following reasons.

1. If in Eq. (3.2) the approximation functional of $\Gamma^{(3)}$ is built in a way that Γ does not necessarily stay positive semidefinite, even though the initial γ and Γ are positive semidefinite. Therefore, regardless of whether the partial trace relation between γ and Γ holds or not, there is no guarantee for γ to be positive semidefinite.

2. If the approximation functional of $\Gamma^{(3)}$ is built in a way that the propagated Γ does stay positive semidefinite (provided the initial γ and Γ are positive semidefinite), but since the Eqs. (3.1) and (3.2) are not compatible and the relation between Γ and γ is ill-defined, the positive-semidefiniteness will not necessarily pass to the γ.

It is not easy to impose positive semidefiniteness on $\Gamma^{(3)}$ and even if we succeed to do that, since its trace relation with γ and Γ is broken this does not lead to the positive semidefiniteness of γ and Γ. In the paper [IV], we used different test approximations to analyze the role of compatibility and positive semidefiniteness in these unphysical results. For example we introduced several approximations which fix the compatibility link between the two equations. That solved the divergence problem only if the approximation was retaining the positive-semidefiniteness as well, and in other cases, the divergence problem still existed.

$\Gamma^{(3)}$ approximations	Compatibility of Equations	Positive-Semidefiniteness of Approximations	Violating ☺ Diverging ☹
$3b - CIF$	✗	✗	☺
$3b - NIA$	✗	✗	☹
WC	✗	✗	☹
Compatible (1)	✓	✓	☺
Compatible (2)	✓	✗	☹
$\left(\frac{N-2}{N}\right)\gamma\,\Gamma$	✗	✗	☺
$3b - NIA$, WC only second equation	Does not Matter	✗	☹
$\left(\frac{N-2}{N}\right)\gamma\,\Gamma$ only second equation	Does not Matter	✓	☺

Table 3.1. Properties and performance of different $\Gamma^{(3)}$ approximations. The test system is a four-electron four-site Hubbard model with fixed Hopping ($t = 1$) and on-site Coulomb energies ($U = 0.1$). Here, m and $\hbar$ are set equal to one. The four electrons filled the two leftmost sites initially.

On the other hand, if we only propagate the second equation (sec. 3.1), even though the compatibility will not be a problem anymore, we can still see diverging results for some of the approximations. Table 3.1 shows an overview of what have been presented in the paper.

3.5 Further truncation schemes

In our paper, we only discussed a few approximations that served our analyses, but what we tried are not limited to those and in fact, there are many other approximations that we tested as a potential cure for the divergence problem but they did not turn out successful. In the following, we provide a list of some of those approximations and their performances in weakly, medium and strongly correlated systems ($U = 0.1, 1$ and 10) in Tables 3.2 and 3.3.

$\Gamma^{(3)}$ approximation	Violating × Non-violating ✓			Diverging × Non-diverging ✓		
	$U = 0.1$	$U = 1$	$U = 10$	$U = 0.1$	$U = 1$	$U = 10$
$3b - CIF$	×	×	×	✓	✓	✓
$3b - NIA$	×	×	×	×	×	×
WC	×	×	×	×	×	×
$3\gamma \wedge \Gamma$	×	×	×	×	×	×
$6\gamma_\Gamma \wedge \gamma_\Gamma \wedge \gamma_\Gamma$	×	×	×	✓	×	×
$-12\gamma_\Gamma \wedge \gamma_\Gamma \wedge \gamma_\Gamma + 9\gamma_\Gamma \wedge \Gamma$	×	×	×	×	×	×
$3\gamma_\Gamma \wedge \Gamma$	×	×	×	×	×	×
$6\gamma_{HF} \wedge \gamma_{HF} \wedge \gamma_{HF}$	×	×	×	✓	✓	✓
$\left(\frac{N-2}{N}\right)\gamma_\Gamma(\mathbf{x}_3, \mathbf{x}_3')\,\Gamma(\mathbf{x}_1\mathbf{x}_2; \mathbf{x}_1'\mathbf{x}_2')$	✓	×	×	✓	✓	✓

Table 3.2. Quality of different $\Gamma^{(3)}$ approximations using both Eqs. (3.1) and (3.2). The test system is a four-electron four-site Hubbard model with fixed Hopping ($t = 1$) and various on-site Coulomb energies (U). γ_Γ in these approximation is given by Eq. (3.3). Here, m and $\hbar$ are set equal to one. The four electrons filled the two leftmost sites initially.

Table 3.2 summarizes different approximations when we propagate both Eq. (3.1) and Eq. (3.2) together. Here, the lack of compatibility between γ and Γ offers another way to use a particular approximation; that is to say, instead of using γ in a $\Gamma^{(3)}$ approximation, we can use γ_Γ defined in Eq. (3.3) and create a distinct but similar approximation. Nevertheless, we still calculate one-body observables from γ and not γ_Γ.

In one of these approximations we used

$$\Gamma^{(3)} = 6\gamma_{HF} \wedge \gamma_{HF} \wedge \gamma_{HF} \tag{3.25}$$

in which we extract the γ_{HF} from the time dependent Hartree-Fock method and feed it here in each time step, namely for this method we need to run the TDHF and BBGKY together and related them in every time step. This approximation is non-diverging for all initial states. Although it violates

the fermionic inequality here, it turned out to be well-behaved for near equilibrium initial states, such as HF ground state or the exact ground state. We are still investigating the quality of the approximation in the linear response regime and for the real systems. Notice that the approximation in the last row of the table is not antisymmetrised with respect to interchange of every two primed or unprimed coordinates separately; however this approximation maintains the essential antisymmetry of Γ.

$\Gamma^{(3)}$ approximation	Violating $\times$			Diverging $\times$		
	Non-violating $\checkmark$			Non-diverging $\checkmark$		
	$U = 0.1$	$U = 1$	$U = 10$	$U = 0.1$	$U = 1$	$U = 10$
$3b - CIF$	$\checkmark$	$\checkmark$	$\checkmark$	$\checkmark$	$\checkmark$	$\checkmark$
$3b - NIA$	$\checkmark$	$\times$	$\times$	$\checkmark$	$\times$	$\times$
WC	$\times$	$\times$	$\times$	$\times$	$\times$	$\times$
$3\,\gamma_\Gamma \wedge \Gamma$	$\times$	$\times$	$\times$	$\times$	$\times$	$\times$
$\left(\frac{N-2}{N}\right)\gamma_\Gamma\left(\mathbf{x}_3, \mathbf{x}_3'\right)\Gamma\left(\mathbf{x}_1\mathbf{x}_2; \mathbf{x}_1'\mathbf{x}_2'\right)$	$\checkmark$	$\checkmark$	$\checkmark$	$\checkmark$	$\checkmark$	$\checkmark$

Table 3.3. Quality of different $\Gamma^{(3)}$ approximations using only Eq. (3.2). The test system is a four-site Hubbard model with fixed Hopping ($t = 1$) and various on-site Coulomb energies (U) and four electrons. Here, γ_Γ (Eq. (3.3)) will be the same as γ. m and $\hbar$ are set equal to one. The four electrons filled the two leftmost sites initially.

In Table 3.3, however, we show the results for the same approximations using only Eq. (3.2) for propagation. This means, as it mentioned in the previous section, γ is the same as γ_Γ even for calculating one-body observables. One should bear in mind that as we showed earlier, the total energy is not constant in any of the approximations used in Table 3.3. Nevertheless, there are two approximations in this table that neither violate the fermionic inequality nor have the divergence problem. We already discussed the quality of the 3b-CIF approximation in the previous section. For other case, i.e. the last-row approximation, we will not go to the detail and only mention that the results are not satisfactory, and they do not describe the system qualitatively.

In short, we provided many test approximations fulfilling different constrains to show that neither compatibility between equations nor positive semidefiniteness of the approximations by itself can keep the propagation of the RDMs inside the fermionic boundaries. In fact, although the nonlinearity introduced by most of the approximations to Eq. (3.2) might be the cause of the divergence, the violation of fermionic inequality might exist even in the case of linear approximations as we saw in the 3b-CIF approximation. Therefore, it indeed takes both of these constraints to tame such

coupled equations.

4. Conclusion

The dissertation was divided into two general parts. First, we applied the DFT-based transport on defective carbon nanotubes, and next, we tried to develop a method for time dependent reduced density matrices.

The first part of the dissertation consists of 3 papers. In the first paper [I] we studied the transmission spectrum of carbon NanoBuds for various geometries and found two common features: the transmission is significantly reduced at E_F and above it, and high-transmission bands exist for energies below E_F. We also showed that the neck region atoms play an important role in the conductance of the system, and suggest that the conductance can be modified by a further manipulation of this region.

Next paper dealt with the effect of multiple bi-site perturbations on electronic and transport properties of armchair nanotubes [II]. Our calculations showed that following a certain relative-position condition, a naturally metallic nanotube can turn into semiconducting. The phenomenon showed robustness against variations in the types of perturbing species and also to some extent in their positions.

In the third work [III] we turned to the nanotube junctions and studied the electronic transport properties of metallic– metallic, semiconducting–semiconducting, and metallic– semiconducting junctions. Our results demonstrated that in the metallic–semiconducting junction a Schottky barrier is formed, affecting the transport. Moreover, when the tubes were close to each other, a charge accumulation effect occurred in the junction area since the p_z orbitals of the carbon atoms start to overlap. We also studied the effect of pressure and doping on the transport properties.

The second part of the dissertation was concerned with the time evolution of reduced density matrices. We focused on the first two equations of the BBGKY hierarchy as our main framework and employed the cluster expansion to approximate the three-body RDM in the second equation.

We showed that by using the first two equations, the total energy of the system is conserved. However, maintaining quantities such as energy and number of particles did not help in obtaining sound results, and in fact using the existing approximation has led to very unphysical (in most cases diverging) behavior. Our thorough analysis and tests also revealed the important role of positive semidefiniteness which a good approximations must maintain.

Bibliography

[1] P. Hohenberg and W. Kohn. Inhomogeneous electron gas. *Phys. Rev.*, 136:B864–B871, 1964.

[2] W. Kohn and L. J. Sham. Self-consistent equations including exchange and correlation effects. *Phys. Rev.*, 140:A1133–A1138, 1965.

[3] J. P. Perdew, K. Burke, and M. Ernzerhof. Generalized gradient approximation made simple. *Phys. Rev. Lett.*, 77:3865–3868, 1996.

[4] A. J. Coleman. Structure of fermion density matrices. *Rev. Mod. Phys.*, 35(3):668–686, 1963.

[5] U. von Barth and L. Hedin. A local exchange-correlation potential for the spin polarized case. i. *Journal of Physics C: Solid State Physics*, 5(13):1629, 1972.

[6] *Phys. Rev. B*, 12.

[7] A. M. K. Müller. Explicit approximate relation between reduced two- and one-particle density matrices. *Physics Letters A*, 105(9):446 – 452, 1984.

[8] M. A. Buijse and E. J. Baerends. An approximate exchange-correlation hole density as a functional of the natural orbitals. *Molecular Physics*, 100(4):401–421, 2002.

[9] O. Gritsenko, K. Pernal, and E. J. Baerends. An improved density matrix functional by physically motivated repulsive corrections. *The Journal of Chemical Physics*, 122(20):204102, 2005.

[10] J. Cioslowski, P. Ziesche, and K. Pernal. On the exactness of simple natural spin-orbital functionals for a high-density homogeneous electron gas. *Phys. Rev. B*, 63:205105, 2001.

[11] N. N. Lathiotakis, N. Helbig, and E. K. U. Gross. Open shells in reduced-density-matrix-functional theory. *Phys. Rev. A*, 72:030501, 2005.

[12] S. Goedecker and C. J. Umrigar. Natural orbital functional for the many-electron problem. *Phys. Rev. Lett.*, 81:866–869, 1998.

[13] A. Holas. Properties of the goedecker-umrigar functional for the many-electron problem and its generalization. *Phys. Rev. A*, 59:3454–3461, 1999.

[14] K. Yasuda. Correlation energy functional in the density-matrix functional theory. *Phys. Rev. A*, 63:032517, 2001.

[15] G. Csányi and T. A. Arias. Tensor product expansions for correlation in quantum many-body systems. *Phys. Rev. B*, 61:7348–7352, 2000.

[16] G. Csányi, S. Goedecker, and T. A. Arias. Improved tensor-product expansions for the two-particle density matrix. *Phys. Rev. A*, 65:032510, 2002.

[17] V. N. Staroverov and G. E. Scuseria. Assessment of simple exchange-correlation energy functionals of the one-particle density matrix. *The Journal of Chemical Physics*, 117(6):2489–2495, 2002.

[18] C. Kollmar and B. A. Hess. A new approach to density matrix functional theory. *The Journal of Chemical Physics*, 119(9):4655–4661, 2003.

[19] P. Leiva and M. Piris. Assessment of a new approach for the two-electron cumulant in natural-orbital-functional theory. *The Journal of Chemical Physics*, 123(21):214102, 2005.

[20] M. Piris. A new approach for the two-electron cumulant in natural orbital functional theory. *International Journal of Quantum Chemistry*, 106(5):1093–1104, 2006.

[21] M. Piris, J. M. Matxain, X. Lopez, and J. M. Ugalde. Spin conserving natural orbital functional theory. *The Journal of Chemical Physics*, 131(2):021102, 2009.

[22] N. N. Lathiotakis, S. Sharma, J. K. Dewhurst, F. G. Eich, M. A. L. Marques, and E. K. U. Gross. Density-matrix-power functional: Performance for finite systems and the homogeneous electron gas. *Phys. Rev. A*, 79:040501, 2009.

[23] M. Piris, J. M. Matxain, X. Lopez, and J. M. Ugalde. Communications: Accurate description of atoms and molecules by natural orbital functional theory. *The Journal of Chemical Physics*, 132(3):031103, 2010.

[24] M. Piris. A natural orbital functional based on an explicit approach of the two-electron cumulant. *International Journal of Quantum Chemistry*, pages n/a–n/a, 2012.

[25] M. Piris. Natural orbital functional theory. In *Reduced-Density-Matrix Mechanics: With Application to Many-Electron Atoms and Molecules*, pages 385–427. John Wiley & Sons, Inc., 2007.

[26] M. Born and H. S. Green. A general kinetic theory of liquids. iv. quantum mechanics of fluids. *Proceedings of the Royal Society of London. Series A. Mathematical and Physical Sciences*, 191(1025):168–181, 1947.

[27] N. N. Bogoliubov. *The dynamical theory in statistical physics*. Hindustan Pub. Corp.(Delhi), 1965.

[28] J.G. Kirkwood. The statistical mechanical theory of transport processes i. general theory. *Journal of Chemical Physics*, 14:180–201, 1946.

[29] J. Yvon. Une méthode d'étude des corrélations dans les fluides quantiques en équilibre. *Nuclear Physics*, 4:1–20, 1957.

[30] M. Bonitz. *Quantum Kinetic Theory*. B.G. Teubner, 1998.

[31] H. Bruus and K. Flensberg. *Many-body quantum theory in condensed matter physics: an introduction*. Oxford University Press, USA, 2004.

[32] M. Koentopp, C. Chang, K. Burke, and R. Car. Density functional calculations of nanoscale conductance. *Journal of Physics: Condensed Matter*, 20(8):083203, 2008.

[33] M. Di Ventra. *Electrical transport in nanoscale systems*. Cambridge University Press, Cambridge, 2008.

[34] G. Stefanucci and C.-O. Almbladh. Time-dependent partition-free approach in resonant tunneling systems. *Phys. Rev. B*, 69:195318, 2004.

[35] G Stefanucci and C.-O. Almbladh. An exact ab initio theory of quantum transport using tddft and nonequilibrium green's functions. *Journal of Physics: Conference Series*, 35(1):17, 2006.

[36] K. S. Thygesen and A. Rubio. Nonequilibrium gw approach to quantum transport in nano-scale contacts. *The Journal of Chemical Physics*, 126(9):091101, 2007.

[37] K. S. Thygesen and A. Rubio. Conserving gw scheme for nonequilibrium quantum transport in molecular contacts. *Phys. Rev. B*, 77(11):115333, 2008.

[38] M. Brandbyge, J. Mozos, P. Ordejón, J. Taylor, and K. Stokbro. Density-functional method for nonequilibrium electron transport. *Phys. Rev. B*, 65(16):165401, 2002.

[39] S. Iijima. Helical microtubules of graphitic carbon. *Nature*, 1991.

[40] A. Hashimoto, K. Suenaga, A. Gloter, K. Urita, and S. Iijima. Direct evidence for atomic defects in graphene layers. *Nature*, 430(7002):870–873, 2004.

[41] J.-C. Charlier, X. Blase, and S. Roche. Electronic and transport properties of nanotubes. *Rev. Mod. Phys.*, 79(2):677, 2007.

[42] K. Balasubramanian and M. Burghard. *Small*, 1:180, 2005.

[43] J. M. García-Lastra, K. S. Thygesen, M. Strange, and A. Rubio. Conductance of sidewall-functionalized carbon nanotubes: Universal dependence on adsorption sites. *Phys. Rev. Lett.*, 101(23):236806, 2008.

[44] A. López-Bezanilla, F. Triozon, S. Latil, X. Blase, and S. Roche. Effect of the chemical functionalization of charge transport in carbon nanotubes at the mesoscopic scale. *Nano Letters*, 9(3):940–944, 2009.

[45] A. G. Nasibulin, P. V. Pikhitsa, H. Jiang, D. P. Brown, A. V. Krasheninnikov, A. S. Anisimov, P. Queipo, A. Moisala, D. Gonzalez, G. Lientschnig, A. Hassanien, S. D. Shandakov, G. Lolli, D. E. Resasco, M. Choi, D. Tomanek, and E. I. Kauppinen. A novel hybrid carbon material. *Nature Nanotech.*, 2(3):156–161, 2007.

[46] R. C. Haddon. Chemistry of the Fullerenes: The Manifestation of Strain in a Class of Continuous Aromatic Molecules. *Science*, 261(5128):1545–1550, 1993.

[47] F. Diederich and C. Thilgen. Covalent Fullerene Chemistry. *Science*, 271(5247):317–324, 1996.

47

[48] A. G. Nasibulin, A. S. Anisimov, P. V. Pikhitsa, H. Jiang, D. P. Brown, M. Choi, and E. I. Kauppinen. Investigations of nanobud formation. *Chem. Phys. Lett.*, 446(1-3):109 – 114, 2007.

[49] P. Havu, A. Sillanpää, N. Runeberg, J. Tarus, E. T. Seppälä, and R. M. Nieminen. Effects of chemical functionalization on electronic transport in carbon nanobuds. *Phys. Rev. B*, 85:115446, 2012.

[50] T. T. Vehviläinen, M. G. Ganchenkova, V. A. Borodin, and R. M. Nieminen. Multiscale study of hydrogen diffusion and clustering on carbon nanotube. *Journal of Nanoscience and Nanotechnology*, 9(7):4246–4253, 2009.

[51] Zh. Zhang and K. Cho. Ab initio study of hydrogen interaction with pure and nitrogen-doped carbon nanotubes. *Phys. Rev. B*, 75(7):075420, 2007.

[52] M. Khazaei, M. Saeed Bahramy, A. Ranjbar, H. Mizuseki, and Y. Kawazoe. Geometrical indications of adsorbed hydrogen atoms on graphite producing star and ellipsoidal like features in scanning tunneling microscopy images: Ab initio study. *Carbon*, 47(14):3306 – 3312, 2009.

[53] R. Saito, G. Dresselhaus, M.S. Dresselhaus, et al. *Physical properties of carbon nanotubes*. Imperial college press London, 1999.

[54] H. W. Ch. Postma, M. de Jonge, Zh. Yao, and C. Dekker. Electrical transport through carbon nanotube junctions created by mechanical manipulation. *Phys. Rev. B*, 62(16):R10653–R10656, 2000.

[55] T. Nakanishi and T. Ando. Conductance of crossed carbon nanotubes. *Journal of the Physical Society of Japan*, 70(6):1647–1658, 2001.

[56] V. Margulis and M. Pyataev. Electron transport in crossed nanotubes with a point contact. *Phys. Rev. B*, 76(8):085411, 2007.

[57] P. N. Nirmalraj, P. E. Lyons, S. De, J. N. Coleman, and J. J. Boland. Electrical connectivity in single-walled carbon nanotube networks. *Nano Lett.*, 9(11):3890–3895, 2009.

[58] M. S. Fuhrer, J. Nygård, L. Shih, M. Forero, Young-Gui Yoon, M. S. C. Mazzoni, Hyoung Joon Choi, Jisoon Ihm, Steven G. Louie, A. Zettl, and Paul L. McEuen. Crossed nanotube junctions. *Science*, 288(5465):494–497, 2000.

[59] B. Gao, A. Komnik, R. Egger, D. C. Glattli, and A. Bachtold. Evidence for luttinger-liquid behavior in crossed metallic single-wall nanotubes. *Phys. Rev. Lett.*, 92(21):216804, 2004.

[60] Y.-G. Yoon, M. S. C. Mazzoni, H. J. Choi, J. Ihm, and S. G. Louie. Structural deformation and intertube conductance of crossed carbon nanotube junctions. *Phys. Rev. Lett.*, 86(4):688–691, 2001.

[61] F. A. Bulat, L. Couchman, and W. Yang. Contact Geometry and Conductance of Crossed Nanotube Junctions under Pressure . *Nano Lett.*, 9(5):1759–1763, 2009.

[62] A. Buldum and J. P. Lu. Contact resistance between carbon nanotubes. *Phys. Rev. B*, 63(16):161403, 2001.

[63] A. Tkatchenko and M. Scheffler. Accurate molecular van der waals inter-
    actions from ground-state electron density and free-atom reference data.
    Phys. Rev. Lett., 102:073005, 2009.

[64] F. Léonard and J. Tersoff. Novel length scales in nanotube devices. *Phys.
    Rev. Lett.*, 83(24):5174–5177, 1999.

[65] F. L. Hirshfeld. . *Theor. Chim. Acta (Berl.)*, 44:129–138, 1977.

[66] S. Dag, R. T. Senger, and S. Ciraci. Theoretical study of crossed and parallel
    carbon nanotube junctions and three-dimensional grid structures. *Phys.
    Rev. B*, 70(20):205407, 2004.

[67] H. Appel and E. K. U. Gross. Time-dependent natural orbitals and occupa-
    tion numbers. *EPL (Europhysics Letters)*, 92(2):23001, 2010.

[68] K. J. Schmitt, P. G. Reinhard, and C. Toepffer. Truncation of time-dependent
    many-body theories. *Zeitschrift für Physik A Hadrons and Nuclei*, 336:123–
    131, 1990.

[69] T. Gherega, R. Krieg, P. G. Reinhard, and C. Toepffer. Dynamics of correla-
    tions in a solvable model. *Nuclear Physics A*, 560(1):166 – 186, 1993.

[70] S. J. Wang and W. Cassing. Explicit treatment of n-body correlations within
    a density-matrix formalism. *Annals of Physics*, 159(2):328 – 350, 1985.

[71] W. Cassing and S. J. Wang. Numerical study of a selfconsistent two-body
    theory for colliding ions in a one-dimensional model. *Zeitschrift für Physik
    A Hadrons and Nuclei*, 328:423–429, 1987.

[72] W. Cassing, K. Niita, and S. J. Wang. Dynamical aspects of intermediate-
    energy nucleus-nucleus collisions. *Zeitschrift für Physik A Hadrons and
    Nuclei*, 331:439–449, 1988.

[73] W. Cassing and A. Pfitzner. Correlation dynamics of finite fermion systems.
    Zeitschrift für Physik A Hadrons and Nuclei, 337:175–183, 1990.

[74] W. Cassing and A. Pfitzner. Self-consistent truncation of the bbgky hier-
    archy on the two-body level. *Zeitschrift für Physik A Hadrons and Nuclei*,
    342:161–167, 1992.

[75] *Phys. Rev. A*, 57.

[76] F. Colmenero, C. P. del Valle, and C. Valdemoro. Approximating q-order
    reduced density matrices in terms of the lower-order ones. i. general rela-
    tions. *Phys. Rev. A*, 47(2):971–978, 1993.

[77] H. Nakatsuji and K. Yasuda. Direct determination of the quantum-mechanical
    density matrix using the density equation. *Phys. Rev. Lett.*, 76(7):1039–
    1042, 1996.

[78] D. A. Mazziotti. Pursuit of n-representability for the contracted schrödinger
    equation through density-matrix reconstruction. *Phys. Rev. A*, 60(5):3618–
    3626, 1999.

[79] D. A. Mazziotti. Approximate solution for electron correlation through the
    use of schwinger probes. *Chemical Physics Letters*, 289(5-6):419 – 427, 1998.

[80] L.F. Shampine. *Numerical solution of ordinary differential equations*. Chapman & Hall, 1994.

[81] D. A. Mazziotti. Anti-hermitian contracted schrödinger equation: Direct determination of the two-electron reduced density matrices of many-electron molecules. *Phys. Rev. Lett.*, 97(14):143002, 2006.

[82] K. J. Schmitt. particle correlations in the mckean model. *Journal of Statistical Physics*, 46:283–302, 1987.

[83] R. Krieg, K. J. Schmitt, and C. Toepffer. Particle correlations in the mckean model. *Journal of Statistical Physics*, 57:267–288, 1989.

[84] R. Goldman and E. A. Frieman. Logarithmic density behavior of a nonequilibrium boltzmann gas. *Journal of Mathematical Physics*, 8(7):1410–1426, 1967.

[85] J. R. Dorfman and E. G. D. Cohen. Difficulties in the kinetic theory of dense gases. *Journal of Mathematical Physics*, 8(2):282–297, 1967.

[86] K.-J. Schmitt, P.-G. Reinhard, and C. Toepffer. Approximate treatment of fermion systems: Chaos through truncation. *Phys. Rev. A*, 40(1):474–476, 1989.

[87] K.-J. Schmitt, P.-G. Reinhard, and C. Toepffer. Regular and irregular behavior of trajectories in the time-dependent hartree-fock approximation. *Phys. Rev. A*, 40(10):6061–6068, 1989.

BUSINESS +
ECONOMY

ART +
DESIGN +
ARCHITECTURE

SCIENCE +
TECHNOLOGY

CROSSOVER

DOCTORAL
DISSERTATIONS